NASA Technical Memorandum 74091

# Turbulent Boundary Layers Over Nonstationary Plane Boundaries

Alan T. Roper and Garl L. Gentry, Jr.

FEBRUARY 1978

NASA

NASA Technical Memorandum 74091

# Turbulent Boundary Layers Over Nonstationary Plane Boundaries

Alan T. Roper

Rose-Hulman Institute of Technology
Terre Haute, Indiana

and

Garl L. Gentry, Jr.

Langley Research Center
Hampton, Virginia

National Aeronautics
and Space Administration

**Scientific and Technical
Information Office**

1978

## SUMMARY

Methods of predicting integral parameters and skin-friction coefficients of turbulent boundary layers developing over moving ground planes are evaluated using test information from the Langley V/STOL tunnel. These data were obtained at Reynolds numbers higher than those previously available for evaluating these predictive techniques. The three methods evaluated are (1) relative integral parameter method; (2) relative power law method; and (3) modified law of the wall method.

Methods (1) and (2) can be used to predict moving-ground-plane shape factors with an expected accuracy of ±10 percent. They may also be used to predict moving-ground-plane displacement and momentum thicknesses with lower expected accuracy. This decrease in accuracy can be traced to the failure of approximations upon which these methods are based to prove universal when compared with V/STOL tunnel test results.

Although no attempt is made to establish the accuracy of the local skin-friction coefficients predicted by the various methods, those produced by methods (1) and (2) show a high degree of agreement. The modified law of the wall method predicts a more rapid decrease in skin friction with increasing ratio of ground-plane velocity to free-stream velocity than do methods (1) and (2).

## INTRODUCTION

Turbulent boundary-layer flows developing over nonstationary boundaries are of interest in studies related to a variety of flows including the Ludwieg tube, moving shock waves near solid boundaries, and the near field drag of tube vehicles. It is thus desirable to accurately predict the boundary-layer characteristics and the skin-friction coefficient for such flows.

Since all present methods of turbulent-boundary-layer calculation rely upon empirical information, and since no significant body of such information exists for the moving-ground-plane case (except for refs. 1 to 3), any useful method of prediction must originate from existing stationary-ground-plane methods (ref. 4). Three such methods, (1) relative integral parameter method, (2) relative power law method, and (3) modified law of the wall method, have been proposed in references 1 to 3 and partially verified by tests performed in two Langley Research Center wind tunnels equipped with moving ground belts. The bulk of this test information was obtained at Reynolds numbers less than $2 \times 10^6$. To extend the Reynolds number range and complete the verification of one or more of the proposed methods, the present tests were conducted in the Langley V/STOL tunnel at Reynolds numbers up to $9.2 \times 10^6$. In this report results of the latest series of tests are compared with those predicted by means of the three proposed methods. Where appropriate, results of the lower Reynolds number tests (refs. 1 to 3) are also included in the comparison.

## SYMBOLS

The units used for physical quantities in this report are given in both the International System of Units (SI) and the U.S. Customary Units except that stations on figures are given in SI Units only. Measurements and calculations were made in the U.S. Customary Units.

| | |
|---|---|
| A,B,A',B' | empirically determined constants (eqs. (15) and (18)) |
| $C_f$ | total skin-friction coefficient |
| $C_f(0)$ | stationary-ground-plane total skin-friction coefficient |
| $c_f$ | local skin-friction coefficient |
| $c_f(0)$ | stationary-ground-plane local skin-friction coefficient |
| g(R) | empirically determined polynomial (eq. (6)) |
| H | shape factor, $\delta^*/\theta$ |
| H(0) | stationary-ground-plane shape factor |
| N | reciprocal of power in relative power law formulation (eq. (8)) |
| N(0) | reciprocal of power in stationary-ground-plane power law formulation |
| n | reciprocal of power in power law formulation (eq. (7)) |
| R | velocity ratio (nominal value), $V_B/U$ |
| $R_x$ | Reynolds number based on x and U |
| $R_y$ | Reynolds number based on y and U |
| U | x-component of mean velocity at edge of boundary layer, m/sec (ft/sec) |
| u | local x-component of mean velocity, m/sec (ft/sec) |
| $u_\tau$ | friction velocity, $\sqrt{\tau_o/\rho}$, m/sec (ft/sec) |
| $V_B$ | velocity of ground belt, m/sec (ft/sec) |
| x | longitudinal distance from leading edge of ground belt, m (ft) |
| y | vertical distance from gound belt, cm (in.) |
| $\delta$ | boundary-layer thickness (defined as y at which u/U = 0.99), cm (in.) |

$\delta(0)$ stationary-ground-plane boundary-layer thickness, cm (in.)

$\delta^*$ displacement thickness, $\int_0^\infty \left(1 - \frac{u}{U}\right) dy$, cm (in.)

$\delta^*(0)$ stationary-ground-plane displacement thickness, cm (in.)

$\varepsilon$ error (see eq. (5))

$\eta$ reciprocal of exponent in modified Blasius shear-stress formulation (eq. (13))

$\theta$ momentum thickness, $\int_0^\infty \frac{u}{U}\left(1 - \frac{u}{U}\right) dy$, cm (in.)

$\theta(0)$ stationary-ground-plane momentum thickness, cm (in.)

$\mu$ dynamic viscosity, N-sec/m$^2$ (lbf-sec/ft$^2$)

$\rho$ mass density, kg/m$^3$ (slugs/ft$^3$)

$\tau$ shearing stress, N/m$^2$ (lbf/ft$^2$)

Subscript:

o measured at $y = 0$

A tilde (~) on a symbol indicates a relative velocity or a quantity based upon velocity measured relative to the ground plane; for example,

$$\tilde{\delta}^* = \int_0^\infty \left(1 - \frac{\tilde{u}}{\tilde{U}}\right) dy$$

## DISCUSSION

### Experimental Data

The data presented in this report were obtained in the Langley V/STOL tunnel. The tunnel was fitted with a moving smooth-surface ground belt (representing a moving ground plane) and operated with the tunnel side walls and ceiling in place. Slots fitted in the side walls to allow variable porosity were, however, partially opened. The general arrangement of the test facility is shown in figure 1(a). Velocity profiles were determined from total-pressure measurements obtained with a total-pressure rake composed of 46 separate tubes of 0.127-cm (0.05-in.) diameter. Simultaneous static-pressure measurements were made by means of a separate probe located to one side of the rake and at a nominal height of 4.2 cm (1.65 in.) above the ground belt. The general

arrangement of the total pressure rake is shown in figures 1(b) and 1(c). All pressure data were obtained by means of a rotary valve and pressure transducer arrangement.

The V/STOL tunnel is equipped with a porous suction plate to remove the normal tunnel floor boundary layer ahead of the belt; therefore, boundary layers presented in this report are assumed to originate at the leading edge of the belt. In practice, however, it is not possible to remove the entire tunnel boundary layer. The effects of this incomplete boundary-layer removal are shown for the $R = 1.0$ (nominal) profiles taken in the V/STOL facility in figure 2. Additional disturbances to the flow were caused at the leading edge by the small slot (between the suction plate and the belt) and the natural entrainment of air from this slot by the belt motion. Inaccuracies were encountered for readings taken nearest the belt because of the tendency of the belt to lift slightly when in motion. None of the data are corrected for these effects.

Total-pressure measurements were made at a nominal dynamic pressure of 526.7 Pa (11 $lbf/ft^2$), velocity of 29.3 m/sec (96.00 ft/sec), and Reynolds number per unit length of $1.87 \times 10^6$ per m ($0.57 \times 10^6$ per ft) at stations 1.37 m (4.50 ft), 2.62 m (8.58 ft), 3.35 m (11.00 ft), 4.27 m (14.00 ft), and 5.18 m (17.00 ft) behind the belt leading edge. Tunnel static pressure during testing was nominally atmospheric. For these conditions, the range of test Reynolds numbers was $2.62 \times 10^6 \leqq R_x \leqq 9.21 \times 10^6$. Data were recorded at values of $V_B/U$ of approximately 0, 0.24, 0.48, 0.74, and 1.00.

Throughout the test a periodic unsteadiness in the boundary layer of as much as ±0.8 m/sec (±2.5 ft/sec) was noted in the velocity measurements. No such fluctuations were apparent in the high-velocity central core of the test section where tunnel-center-line velocity varied less than ±0.2 m/sec (±0.50 ft/sec) during any given test. Constant monitoring of ground belt speed failed to reveal fluctuations of a frequency sufficient to explain the periodic unsteadiness observed in the flow. All efforts to find and eliminate the source of the disturbance were unsuccessful. To eliminate errors induced by this flow condition, multiple readings were taken of all pressure measurements as summarized in table I. Velocities quoted in this report are the arithmetic averages of the velocities determined for each of the multiple pressure measurements. This scheme was not totally satisfactory and some of the scatter apparent in the measured velocity profiles is undoubtedly attributable to this source.

Velocity profiles measured during the V/STOL tunnel tests are presented in figure 3; the velocity data are also given in table II. Summaries of the boundary-layer thickness $\delta$ and the integral parameters $\delta^*$, $\theta$, and $H$ determined from the measured data are presented in table III. The variation of the boundary-layer thickness with $V_B/U$ is presented in figure 4. Also displayed for comparison in that figure are results from the lower Reynolds number tests reported in references 1 and 2.

## Theoretical Methods

Brief descriptions are presented of the three methods suggested (refs. 1 and 2) for predicting the development of the turbulent boundary layer over a moving ground plane. Evaluation of each method is based on a comparison with data measured during the V/STOL tunnel tests and, where appropriate, with data from references 1 and 2.

Relative integral parameter method.- This method (see refs. 1 and 2) is based upon the development of expressions for the relative integral parameters, $\tilde{\delta}^*$, $\tilde{\theta}$, and $\tilde{H}$, obtained by replacing the variable $u/U$ in the usual parameter definitions (ref. 4) by

$$\frac{\tilde{u}}{\tilde{U}} = \frac{u - V_B}{U - V_B} = \frac{(u/U) - R}{1 - R} \tag{1}$$

Thus, for example

$$\tilde{\delta}^* = \int_0^\infty \left(1 - \frac{\tilde{u}}{\tilde{U}}\right) dy$$

If the following assumptions (1) $\tilde{H}$ is nearly independent of $R$ and (2) $\theta/\theta(0)$ is some function independent of $x$, say $g(R)$ are adopted, expressions relating to stationary and moving-ground-plane integral parameters can be generated

$$\theta = g(R)\ \theta(0) \tag{2}$$

$$H = \frac{H(0)}{1 + R[H(0) - 1]} \tag{3}$$

$$\delta^* = \frac{H(0)}{1 + R[H(0) - 1]}\ g(R)\ \theta(0) \tag{4}$$

where $g(R)$ is obtained by fitting the measured data.

The accuracy of this method rests ultimately upon the validity of assumptions (1) and (2). Of these two assumptions, the first is the least critical. Errors in predicted values of $H/H(0)$ resulting from deviations in the assumed relation $\tilde{H}/H(0) = 1$ can be expressed as

$$\varepsilon(H/H(0)) = \pm\left|\frac{1 - R}{\left[1 + R(\tilde{H} - 1)\right]^2}\right|\left|\varepsilon(\tilde{H}/H(0))\right| \tag{5}$$

The variation of $\tilde{H}/H(0)$ as a function of $R$ is presented in figure 5 for the three sets of test data. It will be noted that assumption (1) is rather seriously violated ($\varepsilon(\tilde{H}/H(0))$ maximum of the order of $\pm 0.25$). The most serious variations correspond to large values of $R$. However, as the first term of equation (5) is always less than one, it serves to attenuate errors resulting from assumption (1). Further, the magnitude of that attenuation grows with increasing values of $R$. For data in this report, maximum errors in $H/H(0)$ resulting from the assumption $\tilde{H} = H(0)$ are no more than $\pm 10$ percent. These errors correspond to midrange values of $R$. Errors in the determination of $H/H(0)$ also enter into the determination of $\delta^*/\delta^*(0)$. (See eq. (4).)

The accuracy of assumption (2) is more critical as it enters directly (unattenuated) into both the determination of $\theta/\theta(0)$ and $\delta^*/\delta^*(0)$. (See eqs. (2) and (4).) Reference 2 suggested that $g(R)$ could be represented adequately by the expression

$$g(R) = (1 - R)\left[1 - 1.1756R + 0.7863R(1 + R)\right] \tag{6}$$

The variation predicted by equation (6) is displayed in figure 6 together with data from the V/STOL tunnel tests and references 1 and 2. The expression appears to be a reasonable representation of the data, although a greater x-dependence is apparent in the current data than in that of either of the previous tests. Scatter about the predicted variation indicates a spread of approximately $\pm 0.10$ which is nearly uniform across the $R$ range. Some of this scatter is undoubtedly due to the unsteadiness noted in the boundary-layer velocities of the V/STOL tests.

Measured values of $H/H(0)$, $\theta/\theta(0)$, and $\delta^*/\delta^*(0)$ are compared with those predicted from equations (2), (3), and (4) in figure 7. Comparisons between measured and predicted values of $H/H(0)$ are good, the maximum error being less than $\pm 10$ percent. Comparisons for $\delta^*/\delta^*(0)$ and $\theta/\theta(0)$ are poor and reflect the scatter apparent in $g(R)$ (fig. 6).

The additional assumption that $c_f/c_f(0)$ (like $C_f/C_f(0)$) is independent of $x$ allows the local skin-friction coefficients for the stationary and moving-ground-plane flows to be related.

Relative power law method.- The power law method (see ref. 1) depicts the velocity within the boundary layer as

$$\frac{u}{U} = \left(\frac{y}{\delta}\right)^{1/n} \tag{7}$$

where $n$ is a parameter somewhat dependent upon Reynolds number. Examination of existing moving-ground-plane boundary-layer measurements (refs. 1 and 2)

led Roper and Gentry (refs. 1 and 3) to conclude that velocity distributions measured relative to a moving boundary admit to a similar formulation,

$$\frac{\tilde{u}}{\tilde{U}} = \left(\frac{y}{\tilde{\delta}}\right)^{1/N} \tag{8}$$

where $N$ is nearly independent of $V_B/U$. Although data from the current series of tests display more scatter than those of earlier tests (ref. 1), they conform sufficiently to the format suggested by equation (8) to corroborate its validity at least far downstream of the start of the belt (fig. 8).

Slopes of all measured profiles (V/STOL tunnel tests, refs. 1 and 2) are summarized in figure 9 in the forms suggested by both equations (7) and (8). It is important to note that although $n$ is strongly dependent upon $V_B/U$, $N$ is more nearly constant. The primary motivation for the power law formulation is its simplicity. To maintain that simplicity, it appears desirable to set $N = N(0)$ and to accept the resulting inaccuracy implied by the $V_B/U$ dependence apparent in figure 9.

The usual integral parameters can be developed by using their respective definitions and equation (8)

$$\delta^* = \left[(1 - R)\left(\frac{\tilde{\delta}}{\delta(0)}\right)\right]\delta^*(0) \tag{9}$$

$$\theta = \left[(1 - R)\left(\frac{N + 2R}{N}\right)\left(\frac{\tilde{\delta}}{\delta(0)}\right)\right]\theta(0) \tag{10}$$

$$H = \left(\frac{N}{N + 2R}\right)H(0) \tag{11}$$

Once stationary-ground-plane integral parameters have been computed, equations (9), (10), and (11) can be used to predict the corresponding moving-ground-plane values provided a suitable expression for $\tilde{\delta}/\delta(0)$ can be developed. Measured values for $\tilde{\delta}/\delta(0)$ are presented in figure 10. Much scatter is apparent, particularly at large values of $V_B/U$. The scatter is undoubtedly due partially to the inherent difficulty in determining $\tilde{\delta}$ and $\delta$ accurately, and, for the V/STOL series of tests, is aggravated by the unsteadiness encountered in the boundary layer.

Measured values of $\tilde{\delta}/\delta(0)$ and the values of $N(0)$ obtained from least-squares fits of the stationary-ground-plane logarithmic profiles were used with equations (9), (10), and (11) to compute $\delta^*/\delta^*(0)$, $\theta/\theta(0)$, and $H/H(0)$. These predicted values are compared with the experimentally determined ratios

in figure 11. Comparisons did not appear to be impressive but were acceptable and display increasing accuracy of prediction as the longitudinal distance from the belt leading edge increased.

For incompressible turbulent flow past a semi-infinite flat plate, Blasius (ref. 4) gives the variation of $\tau_o$ with $\delta$ as

$$\frac{\tau_o}{\rho U^2} = 0.0225\left(\frac{\mu}{\rho U \delta}\right)^{1/4} \tag{12}$$

Extending equation (12) to include relative velocity (ref. 5), replacing 1/4 by $1/\eta$, and rearranging yield the expression for local skin-friction coefficient (ref. 1)

$$\frac{c_f}{2} = \frac{\tau_o}{\rho U^2} = 0.0225(1 - R)^{\frac{2\eta-1}{\eta}}\left(\frac{\mu}{\rho U \delta}\right)^{1/\eta} \tag{13}$$

where $R \leq 1$. Equation (13) can be used to predict the local skin-friction coefficient for moving-ground-plane flows once the parameter $\eta$ has been determined. Substitution of equation (13) into the integral form of the momentum equation for a flat-plate zero-pressure-gradient boundary layer, integration, and rearrangement of the results produce the expression

$$\delta = \left(\frac{0.0225}{\theta/\delta}\,\frac{\eta + 1}{\eta}\right)^{\frac{\eta}{\eta+1}}(1 - R)^{\frac{2\eta-1}{\eta+1}}\left(\frac{1}{R_x}\right)^{\frac{1}{\eta+1}} x \tag{14}$$

By using measured values of $\delta$ and $\theta/\delta$ and appropriate values of the various test conditions, equation (14) can be solved numerically for the values of $\eta$. These results are presented in figure 12 for both the present V/STOL tunnel tests and those of reference 1. The variation of $\eta/\eta(0)$ from both series of tests is consistent. Equation (14) was solved for $c_f$ by using computed values of $\eta$. The resulting local skin-friction coefficients are presented in figure 13 together with results from reference 1. With the exception of a single data point from the latest tests, scatter in the predicted value of $c_f$ as a function of $V_B/U$ is less than ±13 percent.

Modified law of the wall method.- The final approach suggested in reference 1 is based upon the hypothesis that the relative velocity profiles obey the law of the wall in the modified form

$$\frac{\tilde{u}}{\tilde{u}_\tau} = A \log\left(\frac{\rho y \tilde{u}_\tau}{\mu}\right) + B \tag{15}$$

where $A = 5.75$, $B = 5.20$, and

$$\tilde{u}_\tau = \sqrt{\frac{\tau_o}{\rho}} = \tilde{U}\sqrt{\frac{\tilde{c}_f}{2}} \tag{16}$$

The local skin-friction coefficient based upon absolute velocity is related to that based upon relative velocity by the equation

$$\frac{c_f}{2} = (1 - R)^2 \frac{\tilde{c}_f}{2} \tag{17}$$

Adopting the formulation suggested by Clauser (ref. 6), equation (15) can be rewritten as

$$\frac{\tilde{u}}{\tilde{U}} = A' \log (\tilde{R}_y) + B' \tag{18}$$

where $A'$ and $B'$ are functions of $A$, $B$, and $c_f$. Charts constructed for a range of $\tilde{c}_f$ values using equation (17) and measured data from the V/STOL tunnel tests are presented in figure 14. Comparison of measured data with the computed $\tilde{c}_f$ grid is used to determine the value of relative skin-friction coefficient.

Although some of the profiles lack a clearly defined linear portion, it was nonetheless possible to determine approximate values of $\tilde{c}_f$ for all stations except $x = 2.62$ m (8.58 ft). Values of $c_f$ determined in the manner just outlined are presented in figure 15. Also displayed in that figure are the results reported in reference 1. Agreement between results for the two sets of measured data is good, maximum scatter being less than ±6 percent.

## Comparison of Local Skin-Friction Coefficients

The relative integral parameter method, relative power law, and modified law of the wall methods all yield means for predicting local skin-friction coefficient. The local skin-friction coefficient is an extremely difficult quantity to measure directly over a moving ground plane and no attempt has been made to establish the accuracy of the various methods. Results from both the V/STOL tunnel tests and those presented in reference 1 are displayed in figure 16. Note that predictions of the relative integral parameter and power law methods agree within less than ±6 percent. Values of $c_f$ predicted by the modified law of the wall method are generally lower than those of the other methods.

## Comparison of Predicted and Measured Integral Parameters

In this section comparisons are made of measured values of $\delta^*/\delta^*(0)$, $\theta/\theta(0)$, and $H/H(0)$ with those predicted by the relative integral parameter and power law methods. Where available, data from the lower Reynolds number tests as well as from the V/STOL tunnel tests are displayed.

Shape factor parameter ($H/H(0)$).- Expressions for $H/H(0)$ were developed in the relative integral parameter (eq. (3)) and relative power law methods (eq. (11)). The first expression contains the approximations that $\tilde{H} = H(0)$, whereas the second approximates the actual value of $N$ by $N(0)$.

The accuracy of equations (3) and (11) is displayed in figure 17 by plotting predicted against measured values of $H/H(0)$. Lines indicating ±10 percent error are included in figure 17. The relative integral parameter method is the somewhat more accurate of the two methods yielding errors from -9 percent to +2 percent. This method generally somewhat underestimates the actual value of the ratio $H/H(0)$. With the exception of four measurements from the current set of tests, the relative power law yields errors from -3 percent to +13 percent. The power law method generally overestimates values of $H/H(0)$.

Momentum thickness parameter ($\theta/\theta(0)$).- Expressions for $\theta/\theta(0)$ were developed in the relative integral parameter (eqs. (2) and (6)) and relative power law methods (eq. (10)). Measured values of $\tilde{\delta}/\delta(0)$ were taken from the curve fitted to the measured data in figure 10.

Once again, the accuracy of equations (2) and (10) is depicted by plotting measured against predicted values of the ratio $\theta/\theta(0)$ (fig. 18). Lines representing ±10 percent and ±20 percent errors are included in that figure. Of the two methods, the relative integral parameter method appears most accurate, 80 percent of the predicted points involving errors of ±20 percent or less and nearly 50 percent of the predictions falling within ±10 percent of the measured value. For the relative power law method, 56 percent of the predicted values are within ±20 percent and 38 percent within ±10 percent of the measured values.

The accuracy of the proposed methods in the determination of $\theta/\theta(0)$ deteriorates markedly from that displayed in the prediction of $H/H(0)$ (fig. 17). This deterioration is due in large part to the failure of the empirical expressions for $g(R)$ and $\tilde{\delta}/\delta(0)$ to accurately represent the experimental data. For the relative power law predictions, the situation is further aggravated by the approximation that $N = N(0)$.

Displacement thickness parameter ($\delta^*/\delta^*(0)$).- Expressions for $\delta^*/\delta^*(0)$ were developed in the relative integral parameter (eq. (4)) and relative power law methods (eq. (9)) where, once again, values of $\tilde{\delta}/\delta(0)$ are taken from a curve fitted to the measured values of that parameter (fig. 10).

The accuracy of equations (4) and (9) is depicted by plotting measured against predicted values of the ratio $\delta^*/\delta^*(0)$ (fig. 19). Lines representing ±10 percent and ±20 percent errors are included in that figure. Each of the two equations predict 60 percent of the measured data points within errors of

less than or equal to ±20 percent. The relative power law method predicts 34 percent of the data points within errors of less than or equal to ±10 percent whereas the integral parameter method predicts only 26 percent within this error band. Overall, there is less dispersion of the error chart data than that displayed in the $\theta/\theta(0)$ chart (fig. 18). Once again, the lack of an accurate match between measured data and the empirical formulations for $g(R)$ and $\tilde{\delta}/\delta(0)$ seems to be the major source of error.

## CONCLUSIONS

The validity of the proposed methods is somewhat clouded by the scatter apparent primarily in the Langley V/STOL tunnel test results presented in this report. This scatter is believed to result from the unsteadiness noted in the boundary-layer velocity measurements for which no explanation is advanced. Nevertheless, the data support the conclusions of NASA TN D-6788, at least far from the leading edge of the moving ground belt. These conclusions are:

1. The velocity profiles measured near a moving ground plane can be described by a relative power law formulation of the form

$$\frac{\tilde{u}}{\tilde{U}} = \left(\frac{y}{\tilde{\delta}}\right)^{1/N}$$

where $\tilde{u}/\tilde{U}$ is the relative velocity ratio, $\tilde{\delta}$ is relative boundary-layer thickness, $y$ is the vertical distance from the ground belt, and $N$ (reciprocal of power) is invariant with ground-plane speed.

2. The integral parameters (displacement thickness $\delta^*$, momentum thickness $\theta$, total skin-friction coefficient $C_f$, and shape factor $H$) can be described with reasonable accuracy by either the relative integral parameter or the relative power law methods.

3. The modified law of the wall method predicts a more rapid decrease in local skin-friction coefficient with increase in belt velocity to free-stream velocity ratio than do either the relative integral parameters or relative power law methods.

As the result of the Langley V/STOL tunnel tests an additional conclusion can be drawn.

4. Although no statement can be made concerning their accuracy, there is a high degree of agreement between the variations of skin-friction ratio $(c_f/c_f(0))$ with momentum thickness ratio $(\theta/\theta(0))$ predicted by the relative integral and relative power law methods.

Langley Research Center
National Aeronautics and Space Administration
Hampton, VA 23665
November 10, 1977

## REFERENCES


1. Roper, Alan T.; and Gentry, Garl L., Jr.: Analysis of a Turbulent Boundary Layer Over a Moving Ground Plane. NASA TN D-6788, 1972.

2. Roper, Alan T.; and Gentry, Garl L., Jr.: Turbulent-Boundary-Layer Development on a Moving Ground Belt of Rough Texture. NASA TM X-2515, 1972.

3. Roper, Alan T.; and Gentry, Garl L.: Growth of Turbulent Boundary Layers Over Nonstationary Boundaries. AIAA J., vol. 12, no. 1, Jan. 1974, pp. 95-96.

4. Schlichting, H.: Lecture Series "Boundary Layer Theory." Part II - Turbulent Flows. NACA TM 1218, 1949.

5. Mirels, Harold: Boundary Layer Behind Shock or Thin Expansion Wave Moving Into Stationary Fluid. NACA TN 3712, 1956.

6. Clauser, Francis H.: Turbulent Boundary Layers in Adverse Pressure Gradients. J. Aeronaut. Sci., vol. 21, no. 2, Feb. 1954, pp. 91-108.

TABLE I.- SUMMARY OF MULTIPLE DATA POINT MEASUREMENTS

| x | | R = $V_B/U$ for - | |
|---|---|---|---|
| m | ft | 10 data points | 30 data points |
| 1.37 | 4.50 | None | 0, 0.245, 0.491, 0.739 |
| 2.62 | 8.58 | 0, 0.243, 0.487 | -, -, -, 0.737 |
| 3.35 | 11.00 | 0, 0.242, - | -, -, 0.492, 0.740 |
| 4.27 | 14.00 | 0, 0.242, 0.486 | None |
| .18 | 17.00 | -, 0.242, 0.484 | 0, -, -, 0.685 |

TABLE II.- DATA FROM BOUNDARY-LAYER SURVEYS

(a) x = 1.37 m (4.50 ft)

| $y/\delta$ | u/U | $y/\delta$ | u/U | $y/\delta$ | u/U | $y/\delta$ | u/U |
|---|---|---|---|---|---|---|---|
| R = 0.00<br>$\delta$ = 2.908 cm (1.145 in.) | | R = 0.245<br>$\delta$ = 2.474 cm (0.974 in.) | | R = 0.491<br>$\delta$ = 2.136 cm (0.841 in.) | | R = 0.739<br>$\delta$ = 2.700 cm (1.063 in.) | |
| 0.0961 | 0.6256 | 0.1129 | 0.6824 | 0.1308 | 0.7920 | 0.1035 | 0.8814 |
| .1659 | .7019 | .1950 | .7536 | .2259 | .8480 | .1788 | .9076 |
| .2096 | .7313 | .2464 | .7914 | .2853 | .8599 | .2258 | .9104 |
| .2707 | .7566 | .3182 | .8116 | .3685 | .8881 | .2916 | .9229 |
| .3231 | .7770 | .3798 | .8392 | .4398 | .9075 | .3481 | .9309 |
| .3580 | .7981 | .4209 | .8489 | .8474 | .9130 | .3857 | .9384 |
| .4104 | .8205 | .4824 | .8664 | .5587 | .9288 | .4422 | .9497 |
| .4628 | .8501 | .5440 | .9029 | .6300 | .9528 | .4986 | .9583 |
| .5065 | .8738 | .5954 | .9251 | .6895 | .9633 | .5457 | .9712 |
| .5589 | .8942 | .6569 | .9290 | .7608 | .9686 | .6021 | .9744 |
| .6026 | .8931 | .7083 | .9425 | .8202 | .9798 | .6492 | .9804 |
| .6637 | .9308 | .7801 | .9646 | .9034 | .9902 | .7150 | .9840 |
| .7161 | .9397 | .8417 | .9713 | .9750 | .9952 | .7714 | .9959 |
| .7859 | .9603 | .9238 | .9852 | 1.0702 | .9999 | .8467 | .9939 |
| .8383 | .9689 | .9856 | .9911 | | | .9031 | .9970 |
| .8995 | .9822 | 1.0575 | .9965 | | | .9690 | 1.0010 |
| .9782 | .9978 | 1.1499 | .9992 | | | 1.0536 | 1.0024 |
| 1.0480 | 1.0004 | | | | | | |

TABLE II.- Continued

(b) x = 2.62 m (8.58 ft)

| y/δ | u/U | y/δ | u/U | y/δ | u/U | y/δ | u/U |
|---|---|---|---|---|---|---|---|
| R = 0.00<br>δ = 4.884 cm (1.924 in.) | | R = 0.243<br>δ = 3.471 cm (1.406 in.) | | R = 0.487<br>δ = 3.129 cm (1.232 in.) | | R = 0.737<br>δ = 3.818 cm (1.503 in.) | |
| 0.0884 | 0.5959 | 0.1210 | 0.6914 | 0.1379 | 0.8294 | 0.0865 | 0.8877 |
| .1300 | .6515 | .1779 | .7502 | .2029 | .8585 | .1331 | .9046 |
| .1663 | .6771 | .2277 | .7776 | .2521 | .8745 | .1730 | .9127 |
| .1871 | .7056 | .2561 | .8015 | .2921 | .8941 | .2195 | .9151 |
| .2235 | .7208 | .3059 | .8216 | .3489 | .9044 | .2528 | .9254 |
| .2243 | .7362 | .3344 | .8348 | .3814 | .9075 | .2794 | .9293 |
| .2807 | .7543 | .3842 | .8562 | .4382 | .9248 | .3127 | .9373 |
| .3223 | .7814 | .4411 | .8632 | .5031 | .9361 | .3659 | .9460 |
| .3743 | .8164 | .5123 | .8918 | .5843 | .9524 | .3925 | .9542 |
| .4107 | .8174 | .5621 | .9119 | .6411 | .9623 | .4324 | .9610 |
| .4418 | .8422 | .6048 | .9170 | .6897 | .9702 | .4790 | .9642 |
| .4782 | .8488 | .6546 | .9352 | .7465 | .9782 | .5123 | .9675 |
| .5094 | .8649 | .6973 | .9488 | .7952 | .9801 | .5522 | .9745 |
| .5510 | .8740 | .7542 | .9555 | .8601 | .9848 | .6121 | .9752 |
| .5822 | .8825 | .7969 | .9515 | .9088 | .9794 | .6520 | .9856 |
| .6186 | .9074 | .8467 | .9703 | .9657 | .9962 | .7119 | .9789 |
| .6602 | .9199 | .9036 | .9810 | 1.0305 | .9966 | .7584 | .9924 |
| .6966 | .9305 | .9534 | .9877 | | | .8117 | .9910 |
| .7589 | .9447 | 1.0388 | .9961 | | | .8782 | .9951 |
| .7953 | .9573 | | | | | .9181 | .9945 |
| .8681 | .9734 | | | | | 1.0112 | .9964 |
| .9253 | .9826 | | | | | | |
| .9980 | .9914 | | | | | | |
| 1.0656 | .9967 | | | | | | |

TABLE II.- Continued

(c) x = 3.35 m (11.00 ft)

| y/δ | u/U | y/δ | u/U | y/δ | u/U | y/δ | u/U |
|---|---|---|---|---|---|---|---|
| R = 0.00<br>δ = 5.794 cm (2.281 in.) | | R = 0.242<br>δ = 4.808 cm (1.893 in.) | | R = 0.492<br>δ = 4.338 cm (1.708 in.) | | R = 0.740<br>δ = 4.333 cm (1.706 in.) | |
| 0.0526 | 0.4749 | 0.0634 | 0.6946 | 0.0761 | 0.7830 | 0.0762 | 0.8859 |
| .0833 | .5952 | .1004 | .7324 | .1171 | .8015 | .1172 | .8979 |
| .1140 | .6316 | .1373 | .7542 | .1406 | .8147 | .1407 | .9049 |
| .1403 | .6678 | .1690 | .7756 | .1757 | .8319 | .1759 | .9070 |
| .1622 | .6910 | .1954 | .7900 | .2050 | .8446 | .2052 | .9233 |
| .1841 | .6929 | .2219 | .8019 | .2284 | .8462 | .2286 | .9228 |
| .2148 | .7129 | .2588 | .8157 | .2577 | .8641 | .2579 | .9296 |
| .2411 | .7316 | .2905 | .8329 | .3045 | .8829 | .3048 | .9362 |
| .2894 | .7603 | .3486 | .8574 | .3631 | .8976 | .3634 | .9512 |
| .3244 | .7694 | .3909 | .8740 | .3982 | .9129 | .3986 | .9526 |
| .3507 | .7925 | .4226 | .8934 | .4451 | .9235 | .4455 | .9583 |
| .3770 | .8019 | .4543 | .8868 | .4744 | .9163 | .4748 | .9637 |
| .4077 | .8190 | .4913 | .9016 | .5154 | .9331 | .5158 | .9656 |
| .4384 | .8389 | .5282 | .9205 | .5681 | .9398 | .5686 | .9724 |
| .4691 | .8340 | .5652 | .9138 | .5974 | .9513 | .5979 | .9758 |
| .4998 | .8570 | .6022 | .9335 | .6442 | .9556 | .6448 | .9822 |
| .5349 | .8672 | .6445 | .9510 | .6911 | .9736 | .6917 | .9876 |
| .5612 | .8793 | .6761 | .9553 | .7379 | .9742 | .7386 | .9885 |
| .6182 | .8941 | .7448 | .9701 | .7965 | .9843 | .7972 | .9862 |
| .6489 | .9114 | .7818 | .9702 | .8433 | .9816 | .8441 | .9897 |
| .7015 | .9266 | .8452 | .9818 | .9136 | .9904 | .9144 | .9924 |
| .7628 | .9393 | .9878 | .9911 | .9898 | .9855 | .9906 | .9914 |
| .8198 | .9618 | 1.0565 | .9939 | 1.0659 | .9920 | 1.0668 | .9933 |
| .9864 | .9867 | 1.1146 | .9971 | | | | |
| 1.0303 | .9875 | | | | | | |
| 1.0829 | .9903 | | | | | | |
| 1.1179 | .9934 | | | | | | |

TABLE II.- Continued

(d) x = 4.27 m (14.00 ft)

| y/δ | u/U | y/δ | u/U | y/δ | u/U |
|---|---|---|---|---|---|
| R = 0.00<br>δ = 8.230 cm (3.240 in.) | | R = 0.242<br>δ = 6.073 cm (2.391 in.) | | R = 0.486<br>δ = 4.641 cm (1.827 in.) | |
| 0.0340 | 0.5593 | 0.0460 | 0.6855 | 0.0602 | 0.7936 |
| .0525 | .6083 | .0711 | .7223 | .0931 | .8123 |
| .0679 | .6369 | .0920 | .7396 | .1204 | .8263 |
| .0833 | .6520 | .1129 | .7549 | .1478 | .8503 |
| .0988 | .6647 | .1338 | .7723 | .1752 | .8599 |
| .1111 | .6845 | .1505 | .7776 | .1971 | .8581 |
| .1296 | .6967 | .1756 | .7917 | .2299 | .8755 |
| .1482 | .7040 | .2007 | .8082 | .2628 | .8849 |
| .1605 | .7221 | .2174 | .8210 | .2847 | .8983 |
| .1852 | .7366 | .2509 | .8281 | .3285 | .9114 |
| .2037 | .7551 | .2760 | .8428 | .3613 | .9162 |
| .2191 | .7619 | .2969 | .8446 | .3887 | .9204 |
| .2438 | .7756 | .3304 | .8628 | .4325 | .9296 |
| .2654 | .7838 | .3596 | .8719 | .4708 | .9356 |
| .2840 | .7899 | .3847 | .8740 | .5036 | .9320 |
| .3087 | .8046 | .4182 | .8971 | .5474 | .9512 |
| .3334 | .8177 | .4516 | .9040 | .5912 | .9619 |
| .3550 | .8276 | .4809 | .9170 | .6296 | .9655 |
| .3920 | .8483 | .5311 | .9232 | .6953 | .9714 |
| .4136 | .8532 | .5603 | .9327 | .7336 | .9755 |
| .4537 | .8734 | .6147 | .9479 | .8047 | .9833 |
| .4939 | .8821 | .6691 | .9576 | .8759 | .9875 |
| .5340 | .8989 | .7234 | .9593 | .9471 | .9907 |
| .5741 | .9112 | .7778 | .9777 | 1.0182 | .9228 |
| .6112 | .9255 | .8280 | .9851 | | |
| .6513 | .9371 | .8823 | .9917 | | |
| .6852 | .9424 | .9283 | .9904 | | |
| .7192 | .9542 | .9743 | .9924 | | |
| .7346 | .9466 | .9952 | .9885 | | |
| .7809 | .9731 | 1.0580 | .9966 | | |
| .8272 | .9807 | | | | |
| .8519 | .9789 | | | | |
| .8982 | .9904 | | | | |
| .9322 | .9902 | | | | |
| .9723 | .9899 | | | | |
| 1.0093 | .9876 | | | | |

TABLE II.- Concluded

(e) x = 5.18 m (17.00 ft)

| y/δ | u/U | y/δ | u/U | y/δ | u/U | y/δ | u/U |
|---|---|---|---|---|---|---|---|
| R = 0.00<br>δ = 8.948 cm (3.523 in.) | | R = 0.242<br>δ = 7.120 cm (2.803 in.) | | R = 0.484<br>δ = 5.321 cm (2.095 in.) | | R = 0.685<br>δ = 5.377 cm (2.117 in.) | |
| 0.0341 | 0.4990 | 0.0392 | 0.6956 | 0.0525 | 0.8033 | 0.0567 | 0.8671 |
| .0539 | .5683 | .0607 | .7255 | .0811 | .8190 | .0898 | .8833 |
| .0681 | .6098 | .0821 | .7419 | .1098 | .8329 | .1134 | .8924 |
| .0795 | .6167 | .0999 | .7521 | .1336 | .8472 | .1323 | .8937 |
| .0937 | .6460 | .1177 | .7622 | .1575 | .8553 | .1559 | .9058 |
| .1192 | .6824 | .1320 | .7723 | .1766 | .8604 | .1748 | .9133 |
| .1703 | .7256 | .1534 | .7841 | .2052 | .8747 | .1984 | .9183 |
| .1873 | .7335 | .1748 | .8046 | .2338 | .8791 | .2362 | .9204 |
| .2072 | .7610 | .1962 | .8148 | .2625 | .8928 | .2834 | .9441 |
| .2242 | .7578 | .2141 | .8262 | .2863 | .8975 | .3118 | .9421 |
| .2413 | .7659 | .2391 | .8365 | .3198 | .9037 | .3449 | .9385 |
| .2640 | .7673 | .2605 | .8440 | .3484 | .9121 | .3732 | .9577 |
| .2839 | .7856 | .2819 | .8589 | .3770 | .9218 | .4015 | .9524 |
| .3037 | .7874 | .3104 | .8616 | .4152 | .9383 | .4393 | .9568 |
| .3264 | .7979 | .3318 | .8588 | .4438 | .9280 | .4724 | .9621 |
| .3548 | .8233 | .3604 | .8807 | .4820 | .9403 | .5055 | .9694 |
| .3804 | .8214 | .3925 | .8910 | .5250 | .9514 | .5433 | .9663 |
| .4002 | .8414 | .4139 | .8980 | .5536 | .9580 | .5905 | .9715 |
| .4371 | .8446 | .4567 | .9040 | .6109 | .9702 | .6330 | .9795 |
| .4712 | .8701 | .4817 | .9204 | .6443 | .9719 | .6661 | .9738 |
| .5053 | .8739 | .5281 | .9212 | .7063 | .9795 | .7275 | .9878 |
| .5422 | .8934 | .5780 | .9381 | .7731 | .9849 | .7842 | .9891 |
| .5762 | .8816 | .6173 | .9474 | .8256 | .9841 | .8408 | .9937 |
| .6131 | .9001 | .6672 | .9632 | .8926 | .9910 | .9022 | .9925 |
| .6784 | .9363 | .7064 | .9696 | .9451 | .9931 | .9589 | .9932 |
| .7068 | .9409 | .7528 | .9787 | 1.0072 | .9919 | 1.0203 | .9943 |
| .7352 | .9561 | .7921 | .9785 | | | | |
| .7778 | .9671 | .8313 | .9823 | | | | |
| .8033 | .9643 | .8492 | .9840 | | | | |
| .8459 | .9687 | .9027 | .9896 | | | | |
| .8771 | .9621 | .9562 | .9930 | | | | |
| .9112 | .9776 | .9848 | .9936 | | | | |
| .9481 | .9829 | 1.0347 | .9916 | | | | |
| .9736 | .9831 | | | | | | |
| 1.0304 | .9938 | | | | | | |

TABLE III.- SUMMARY OF GROSS PARAMETERS FROM PROFILE MEASUREMENTS

| x | | R | U | | R | δ | | δ* | | θ | | H | N |
|---|---|---|---|---|---|---|---|---|---|---|---|---|---|
| m | ft | | m/sec | ft/sec | | cm | in. | cm | in. | cm | in. | | |
| 1.37 | 4.50 | 0.000 | 29.83 | 97.88 | $2.62 \times 10^6$ | 2.908 | 1.145 | 0.472 | 0.186 | 0.236 | 0.093 | 1.998 | 4.887 |
| | | .245 | 29.82 | 97.83 | 2.62 | 2.474 | .974 | .363 | .144 | .226 | .089 | 1.613 | 4.021 |
| | | .491 | 29.82 | 97.84 | 2.62 | 2.136 | .841 | .203 | .080 | .145 | .057 | 1.411 | 3.853 |
| | | .739 | 29.77 | 97.67 | 2.61 | 2.700 | 1.063 | .112 | .044 | .091 | .036 | 1.203 | 3.472 |
| 2.62 | 8.58 | .000 | 30.11 | 98.79 | 4.90 | 4.877 | 1.924 | .919 | .362 | .523 | .206 | 1.754 | 4.662 |
| | | .243 | 30.10 | 98.76 | 4.90 | 3.571 | 1.406 | .561 | .221 | .358 | .141 | 1.564 | 4.209 |
| | | .487 | 30.12 | 98.81 | 4.90 | 3.129 | 1.232 | .290 | .114 | .211 | .083 | 1.376 | 4.886 |
| | | .737 | 29.86 | 97.95 | 5.00 | 3.818 | 1.503 | .208 | .082 | .185 | .073 | 1.120 | 4.071 |
| 3.35 | 11.00 | .000 | 30.24 | 99.20 | 6.24 | 5.794 | 2.281 | 1.130 | .445 | .716 | .282 | 1.576 | 4.500 |
| | | .242 | 30.25 | 99.25 | 6.25 | 4.808 | 1.893 | .635 | .250 | .455 | .179 | 1.398 | 5.071 |
| | | .492 | 29.79 | 97.75 | 6.40 | 4.338 | 1.708 | .490 | .193 | .401 | .158 | 1.221 | 4.267 |
| | | .740 | 29.76 | 97.65 | 6.39 | 4.333 | 1.706 | .297 | .117 | .272 | .107 | 1.088 | 4.133 |
| 4.27 | 14.00 | .000 | 30.25 | 99.23 | 7.91 | 8.230 | 3.240 | 1.313 | .517 | .904 | .356 | 1.449 | 5.727 |
| | | .242 | 30.19 | 99.06 | 7.89 | 6.073 | 2.391 | .767 | .302 | .577 | .227 | 1.329 | 5.523 |
| | | .486 | 30.18 | 99.02 | 7.89 | 4.641 | 1.827 | .419 | .165 | .343 | .135 | 1.220 | 5.205 |
| 5.18 | 17.00 | .000 | 32.10 | 105.32 | 9.21 | 8.948 | 3.523 | 1.529 | .602 | 1.041 | .410 | 1.469 | 5.235 |
| | | .242 | 30.22 | 99.16 | 9.61 | 7.120 | 2.803 | .843 | .332 | .643 | .253 | 1.311 | 5.873 |
| | | .484 | 30.30 | 99.41 | 9.63 | 5.321 | 2.095 | .465 | .183 | .386 | .152 | 1.202 | 5.610 |
| | | .685 | 32.13 | 105.40 | 9.22 | 5.377 | 2.117 | .330 | .130 | .297 | .117 | 1.111 | 5.013 |

TABLE III.- Concluded

| x | | R | $\tilde{\delta}$ | | $\tilde{\delta}^*$ | | $\tilde{\theta}$ | | $\tilde{H}$ |
|---|---|---|---|---|---|---|---|---|---|
| m | ft | | cm | in. | cm | in. | cm | in. | |
| 1.37 | 4.50 | 0.000 | 2.908 | 1.145 | 0.472 | 0.186 | 0.236 | 0.093 | 1.998 |
| | | .245 | 2.421 | .953 | .450 | .177 | .267 | .105 | 1.690 |
| | | .491 | 2.050 | .807 | .330 | .130 | .206 | .081 | 1.606 |
| | | .739 | 2.441 | .961 | .320 | .126 | .178 | .070 | 1.814 |
| 2.62 | 8.58 | .000 | 4.887 | 1.924 | .919 | .362 | .523 | .206 | 1.754 |
| | | .243 | 3.500 | 1.378 | .688 | .271 | .427 | .168 | 1.609 |
| | | .487 | 3.038 | 1.196 | .462 | .182 | .318 | .125 | 1.447 |
| | | .737 | 3.449 | 1.358 | .668 | .263 | .503 | .198 | 1.330 |
| 3.35 | 11.00 | .000 | 5.794 | 2.281 | 1.130 | .445 | .716 | .282 | 1.576 |
| | | .242 | 4.669 | 1.838 | .803 | .316 | .551 | .217 | 1.454 |
| | | .492 | 4.094 | 1.612 | .884 | .348 | .660 | .260 | 1.335 |
| | | .740 | 3.988 | 1.570 | 1.019 | .401 | .820 | .323 | 1.243 |
| 4.27 | 14.00 | .000 | 8.230 | 3.240 | 1.313 | .517 | .904 | .356 | 1.449 |
| | | .242 | 5.865 | 2.309 | .876 | .345 | .706 | .278 | 1.333 |
| | | .486 | 4.379 | 1.724 | .749 | .295 | .564 | .222 | 1.325 |
| 5.18 | 17.00 | .000 | 8.948 | 3.523 | 1.529 | .602 | 1.041 | .410 | 1.469 |
| | | .242 | 6.922 | 2.725 | 1.080 | .425 | .790 | .311 | 1.365 |
| | | .484 | 5.027 | 1.979 | .833 | .328 | .643 | .253 | 1.297 |
| | | .685 | 4.900 | 1.929 | .940 | .370 | .747 | .294 | 1.260 |

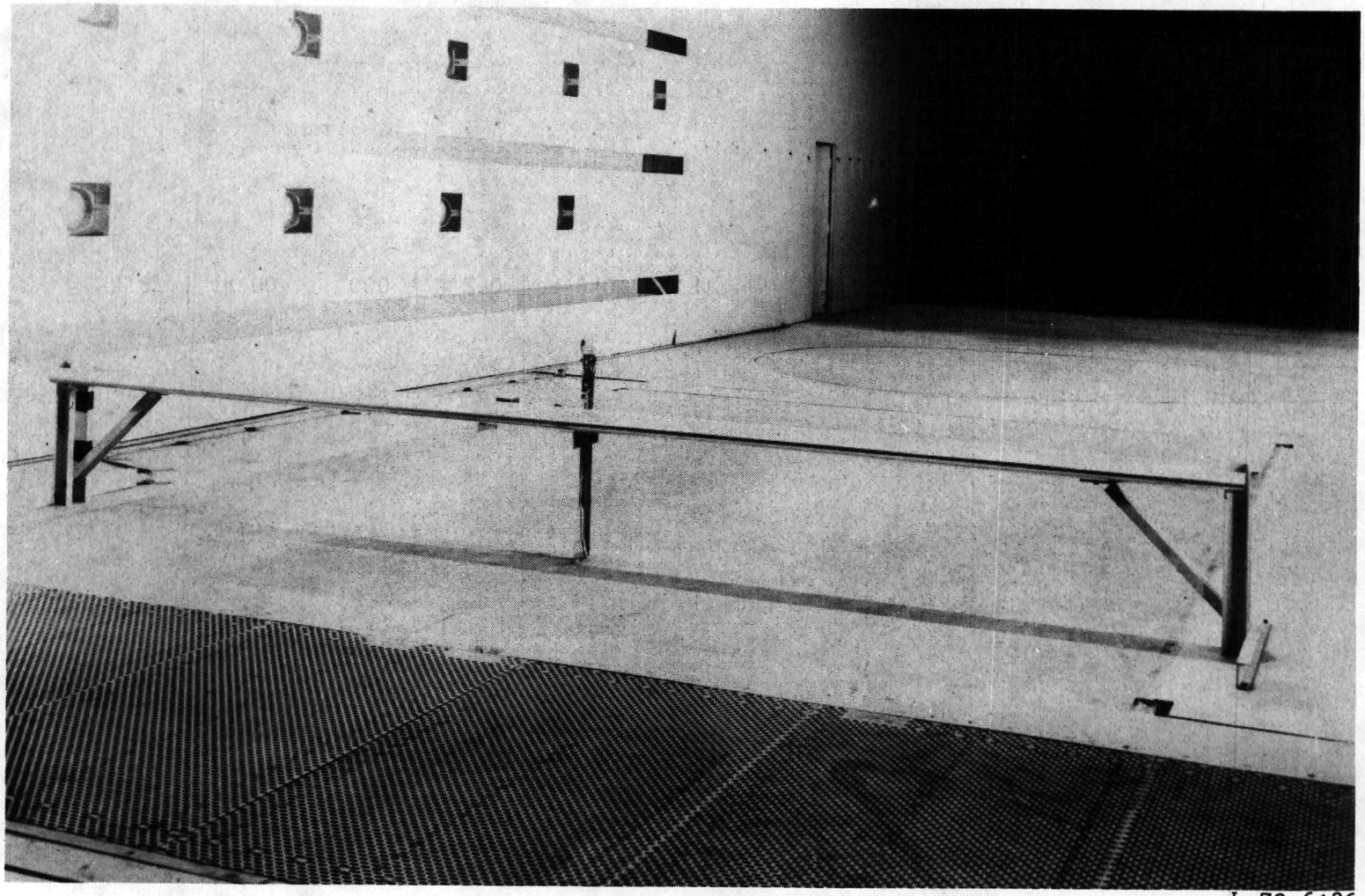

L-73-6186

(a) View from tunnel looking downstream.

Figure 1.- Total-pressure rake and ground-belt arrangement.

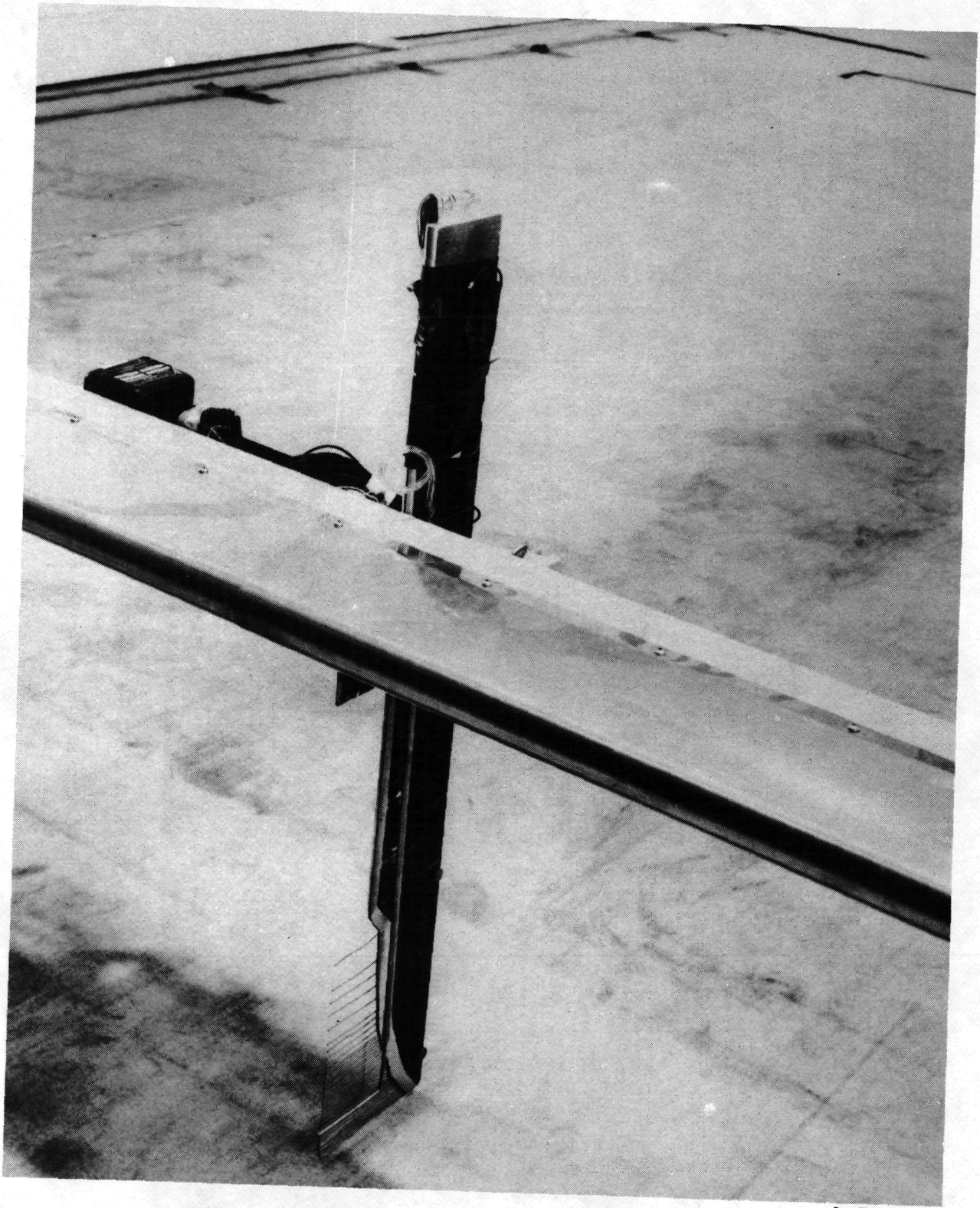

L-73-5263

(b) General arrangement of total-pressure rake at mounting.

Figure 1.- Continued.

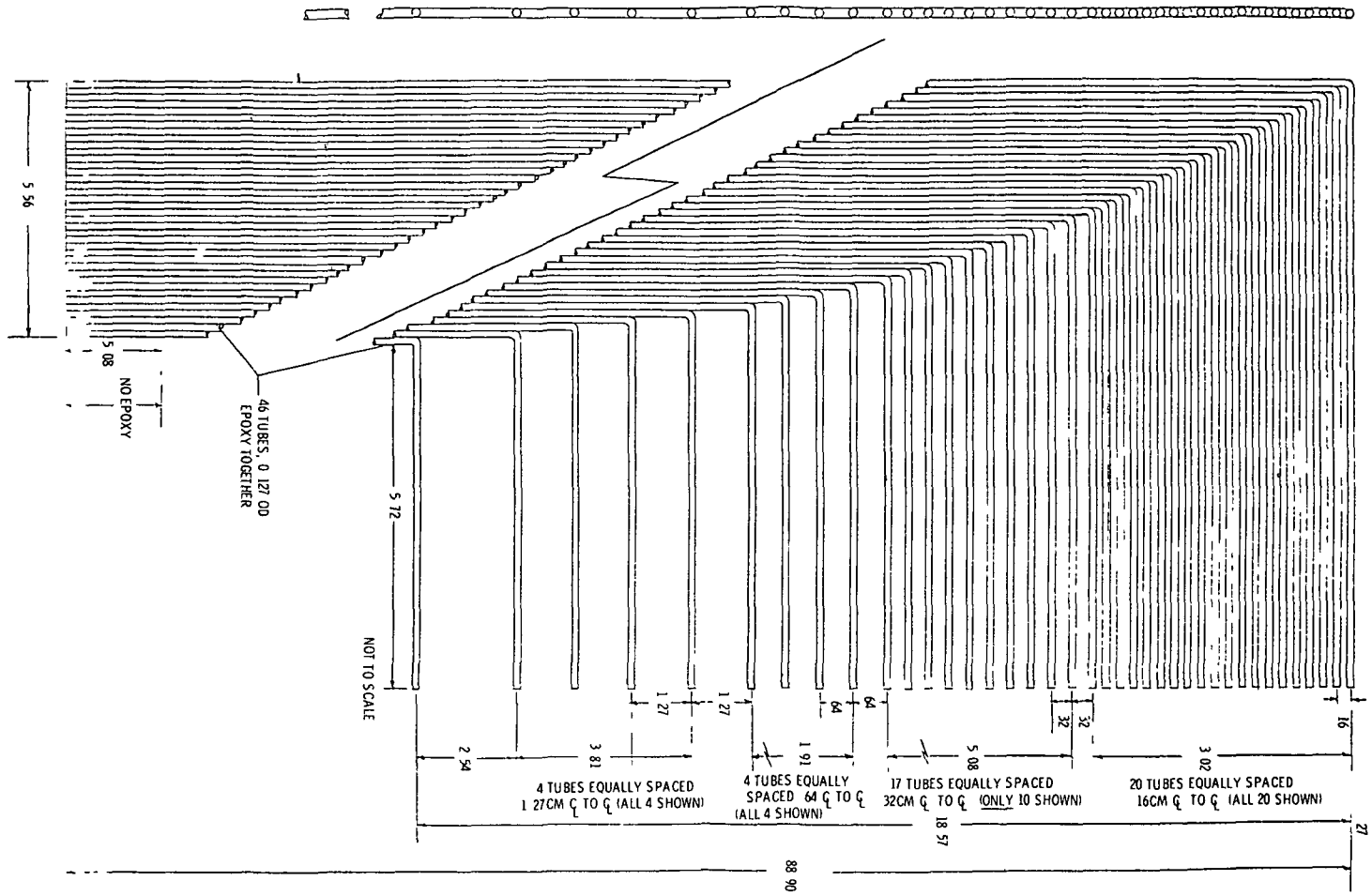


(c) General arrangement of total pressure rake. All dimensions in centimeters.

Figure 1.- Concluded.

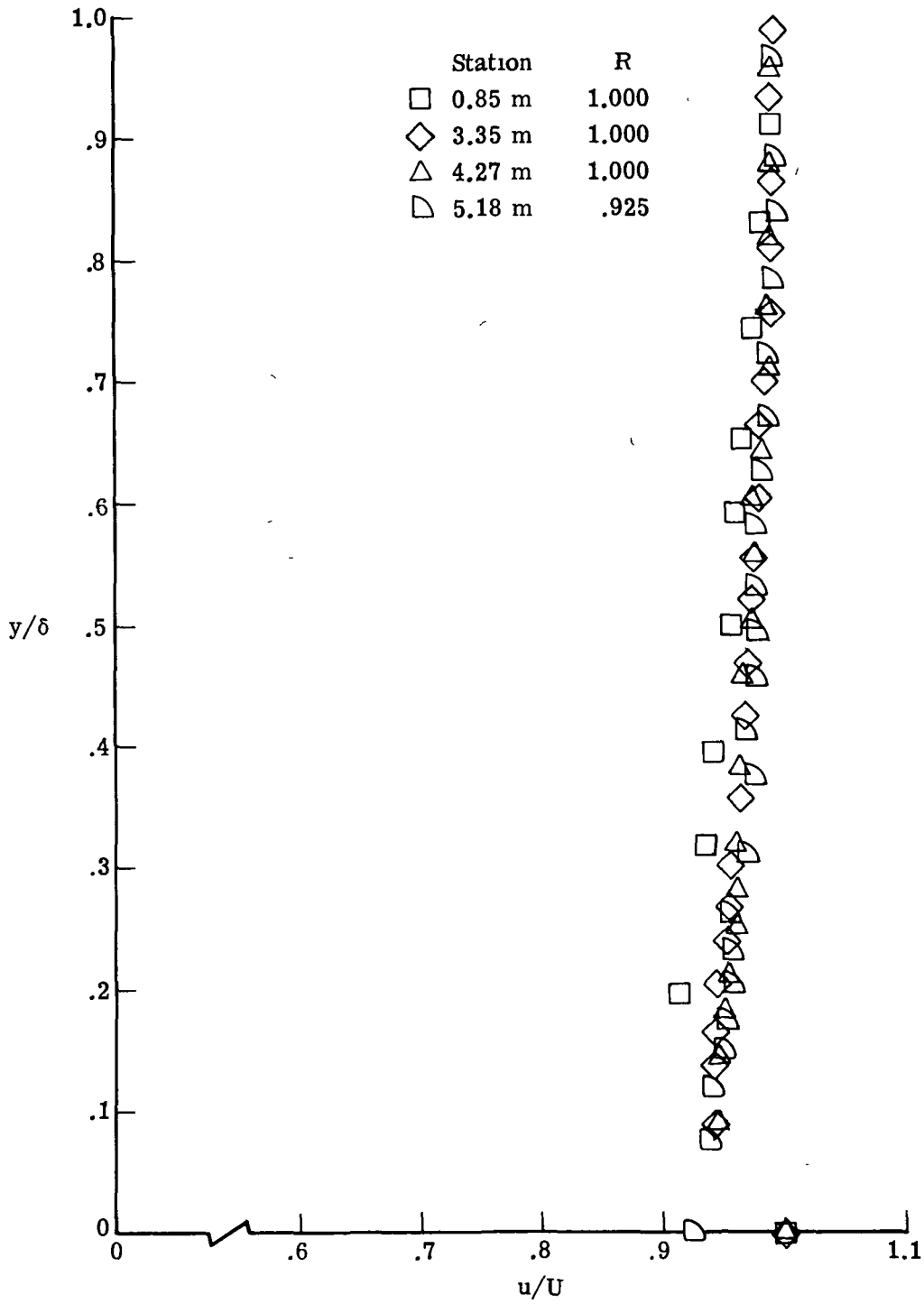


Figure 2.- Velocity profiles displaying effect of incomplete removal of normal wind-tunnel floor boundary layer ahead of moving ground belt.

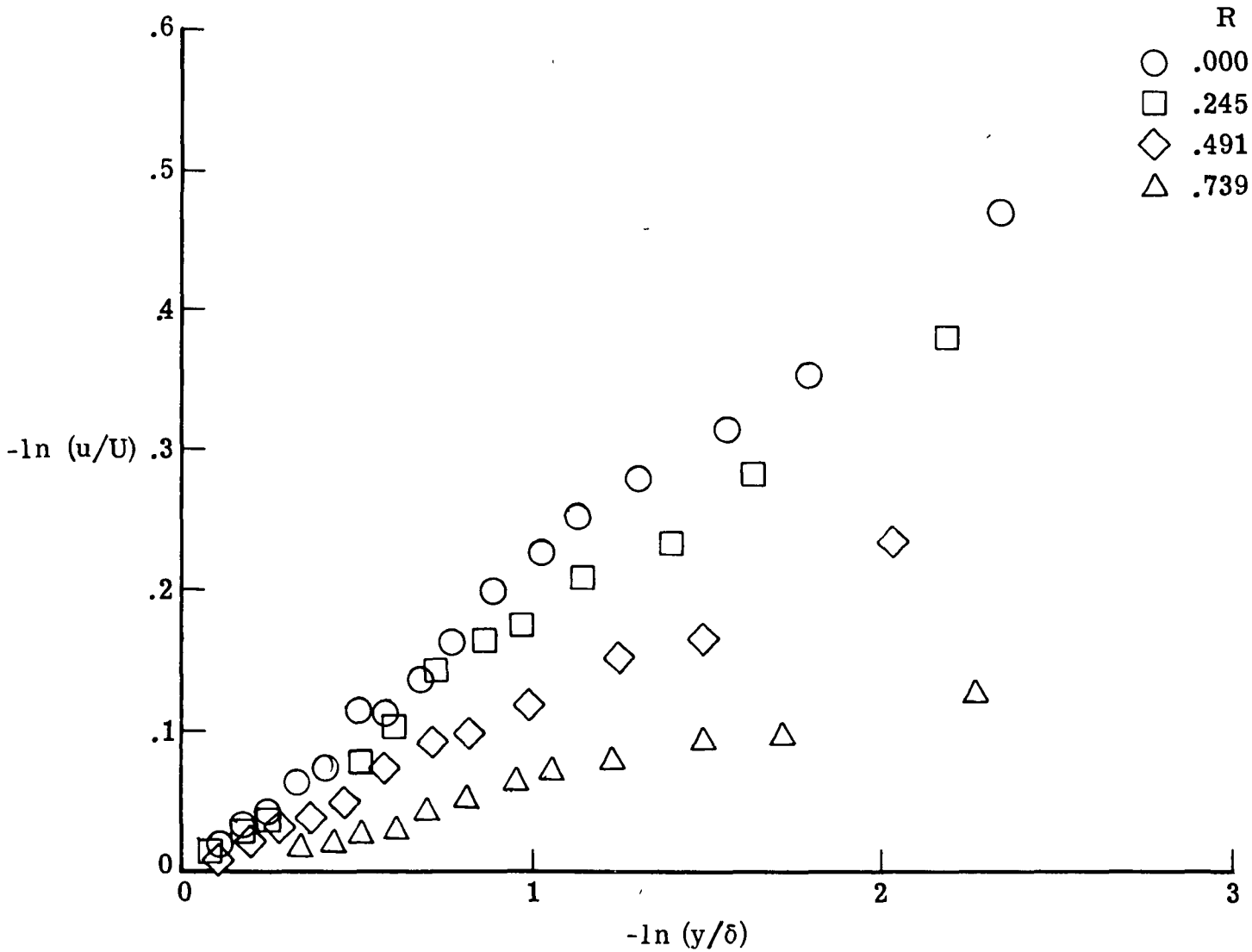


(a) Station x = 1.37 m (4.50 ft).

Figure 3.- Measured velocity profiles.

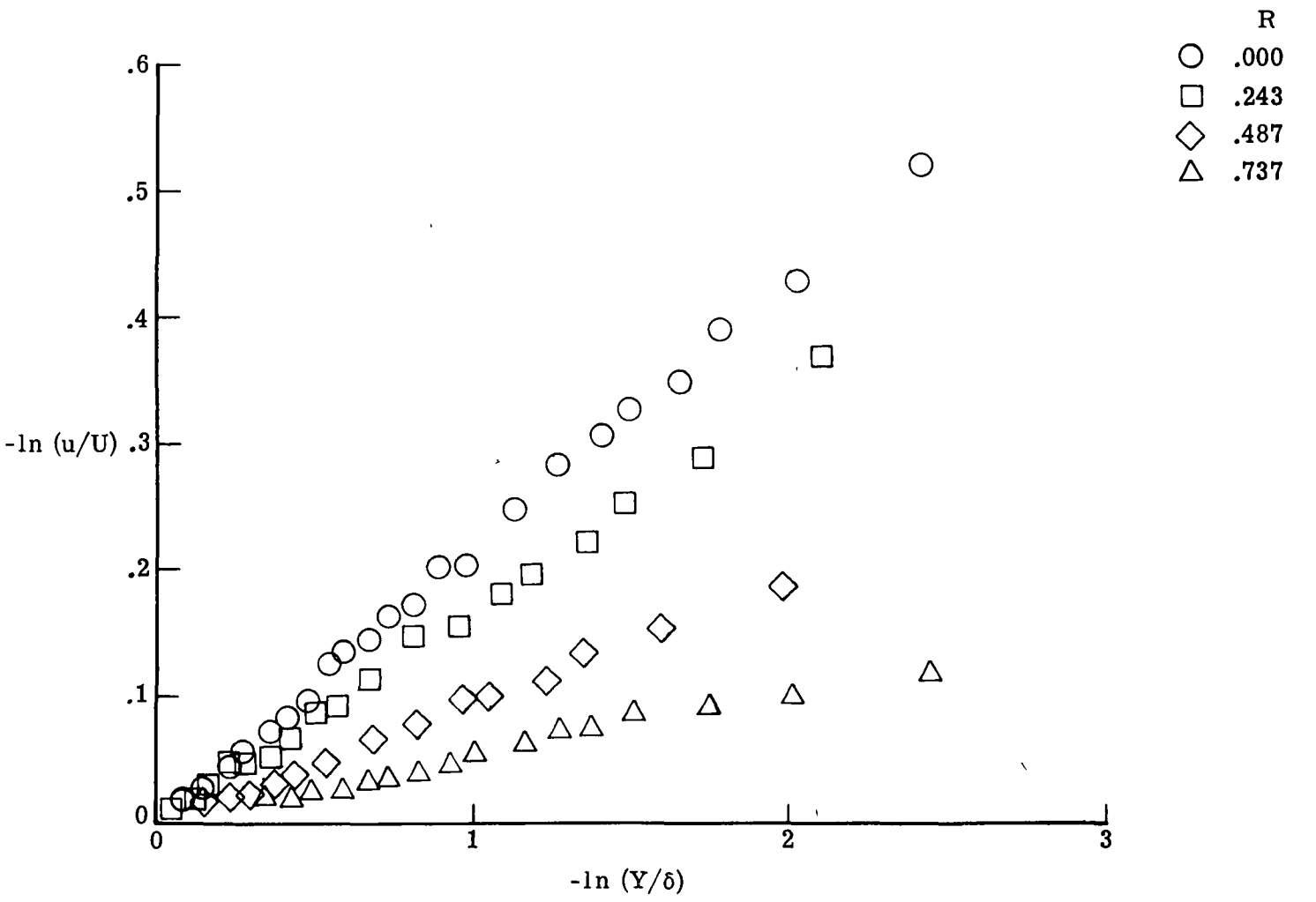


(b) Station x = 2.62 m (8.58 ft).

Figure 3.- Continued.

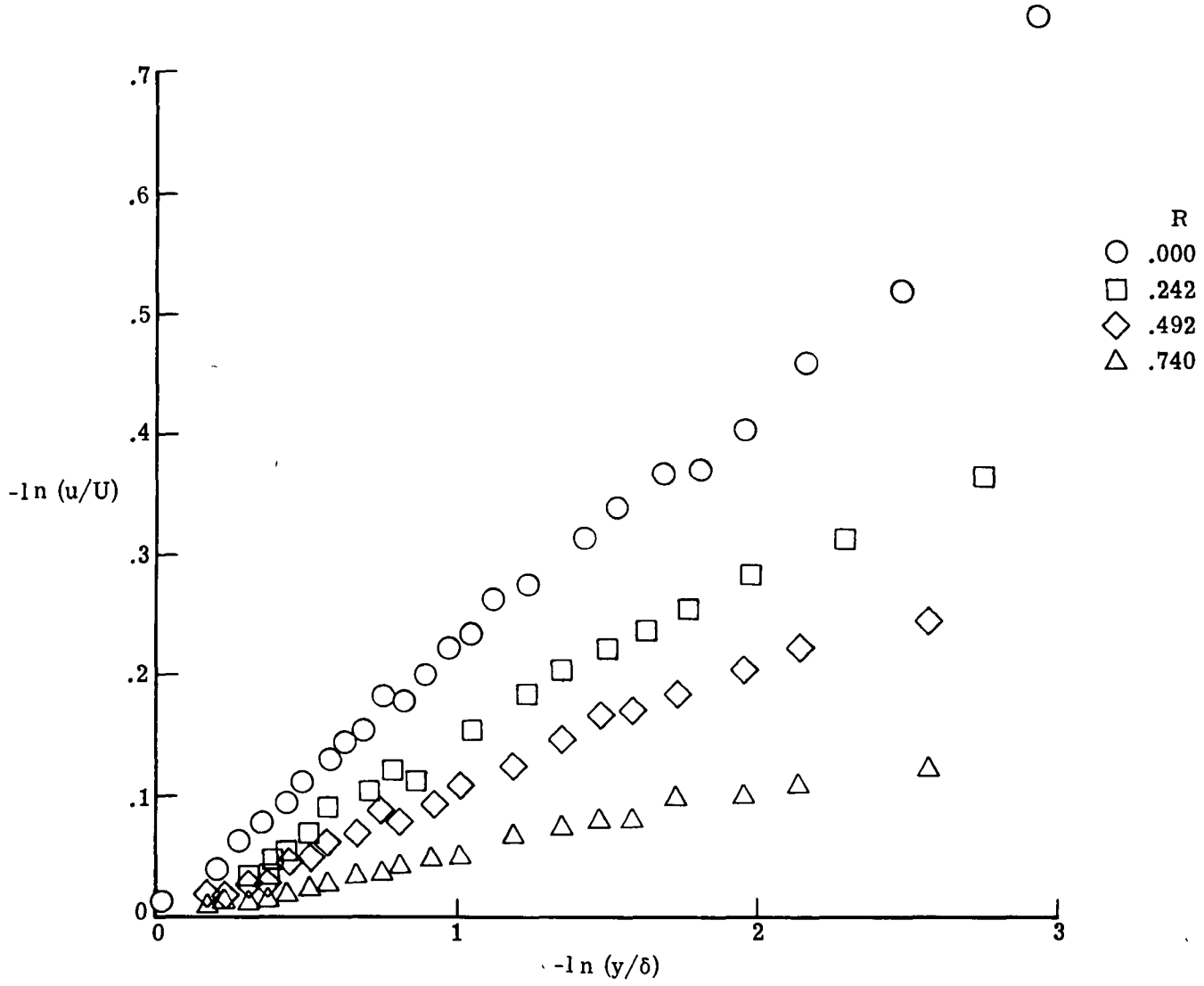


(c) Station x = 3.35 m (11.00 ft).

Figure 3.- Continued.

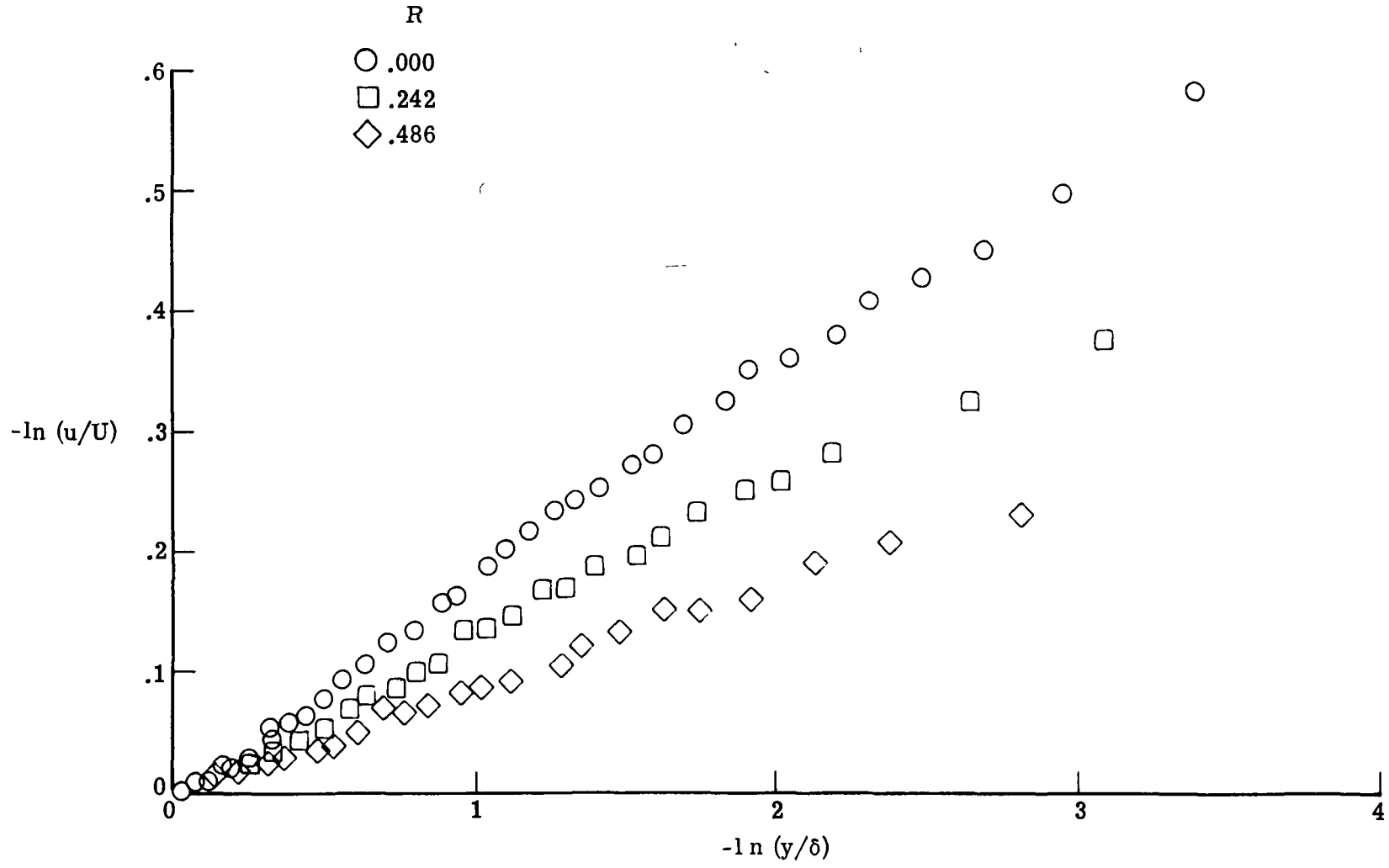


(d) Station x = 4.27 m (14.00 ft).

Figure 3.- Continued.

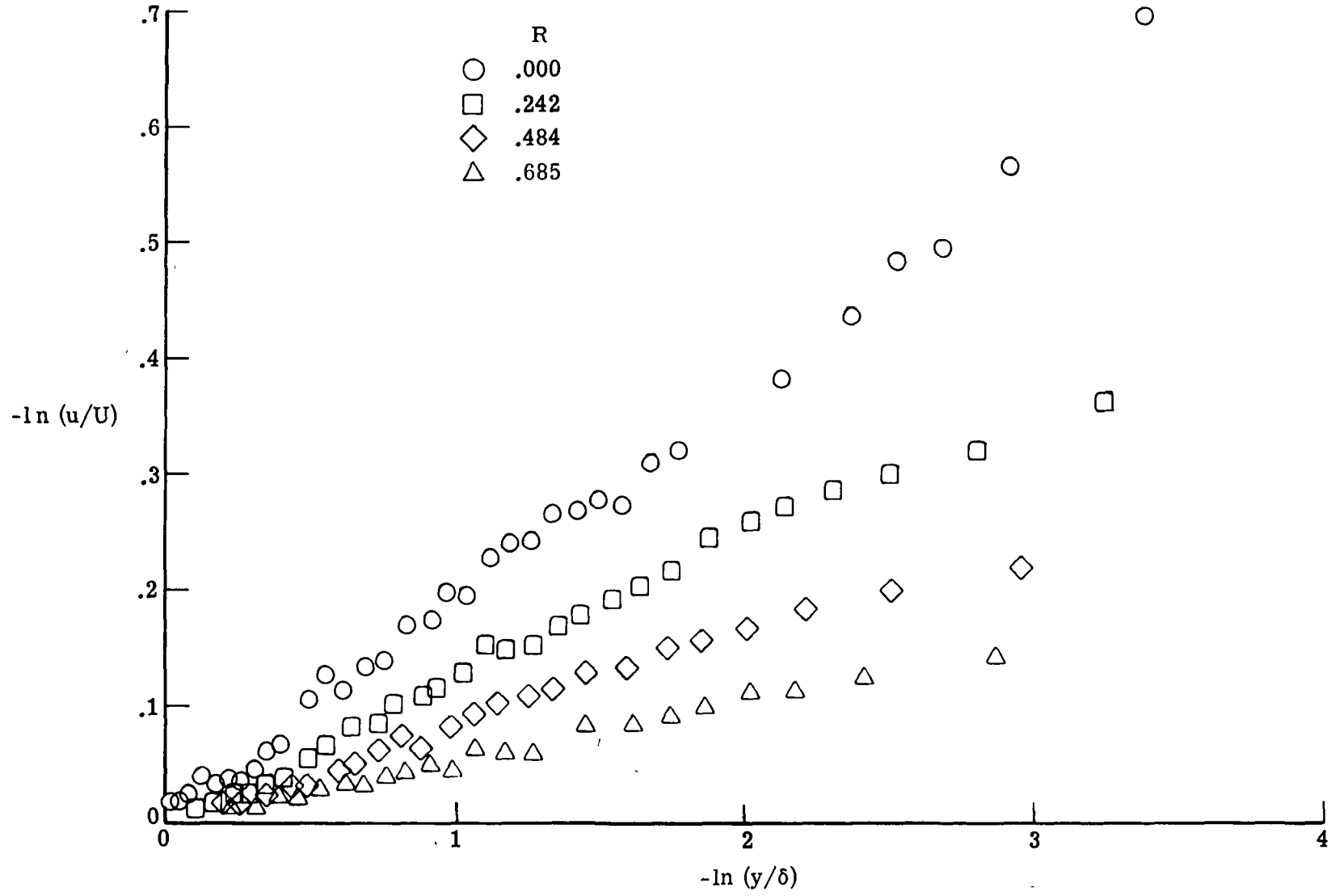


(e) Station x = 5.18 m (17.00 ft).

Figure 3.- Concluded.

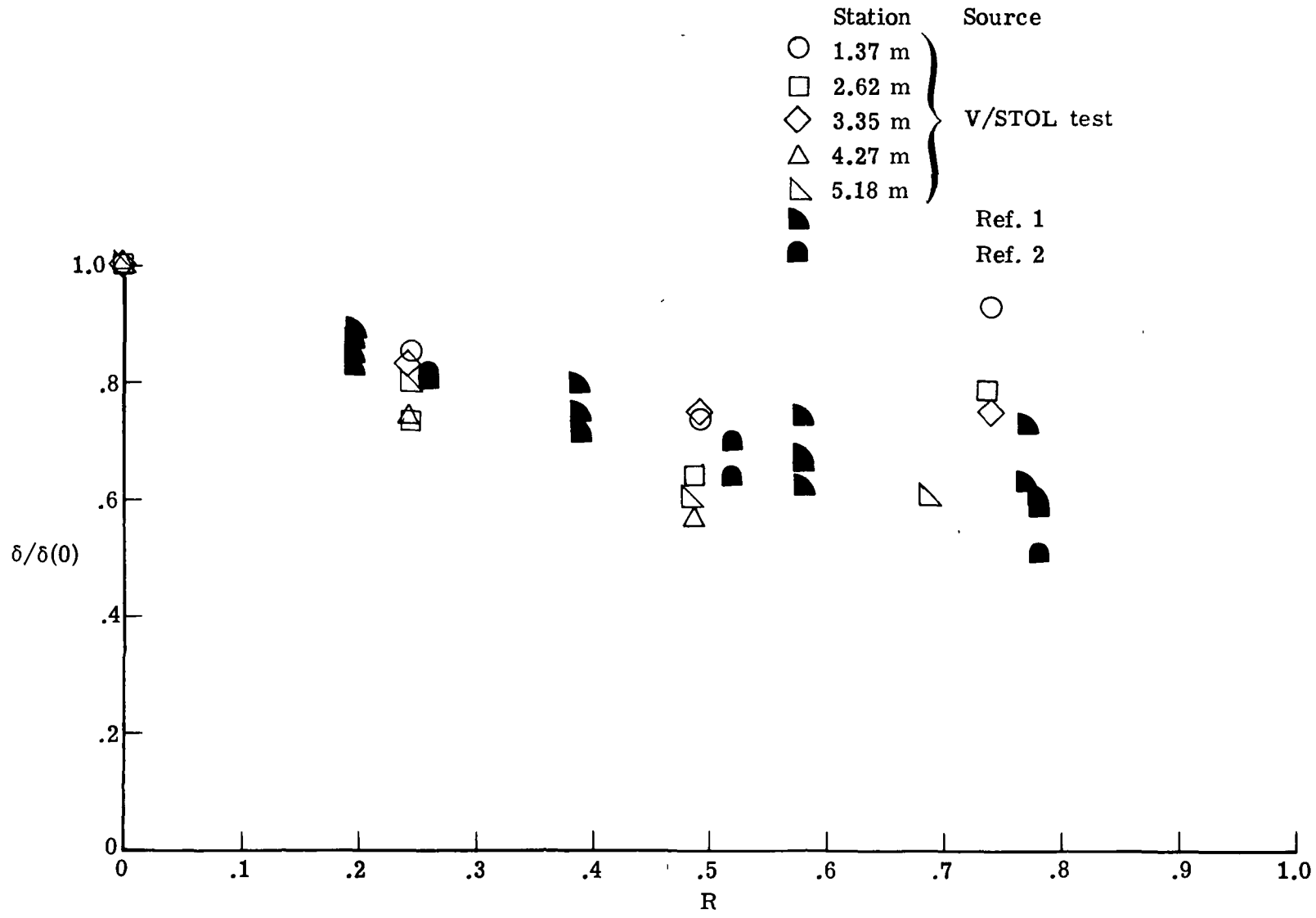


Figure 4.- Variation of boundary-layer thickness with ground-plane speed.

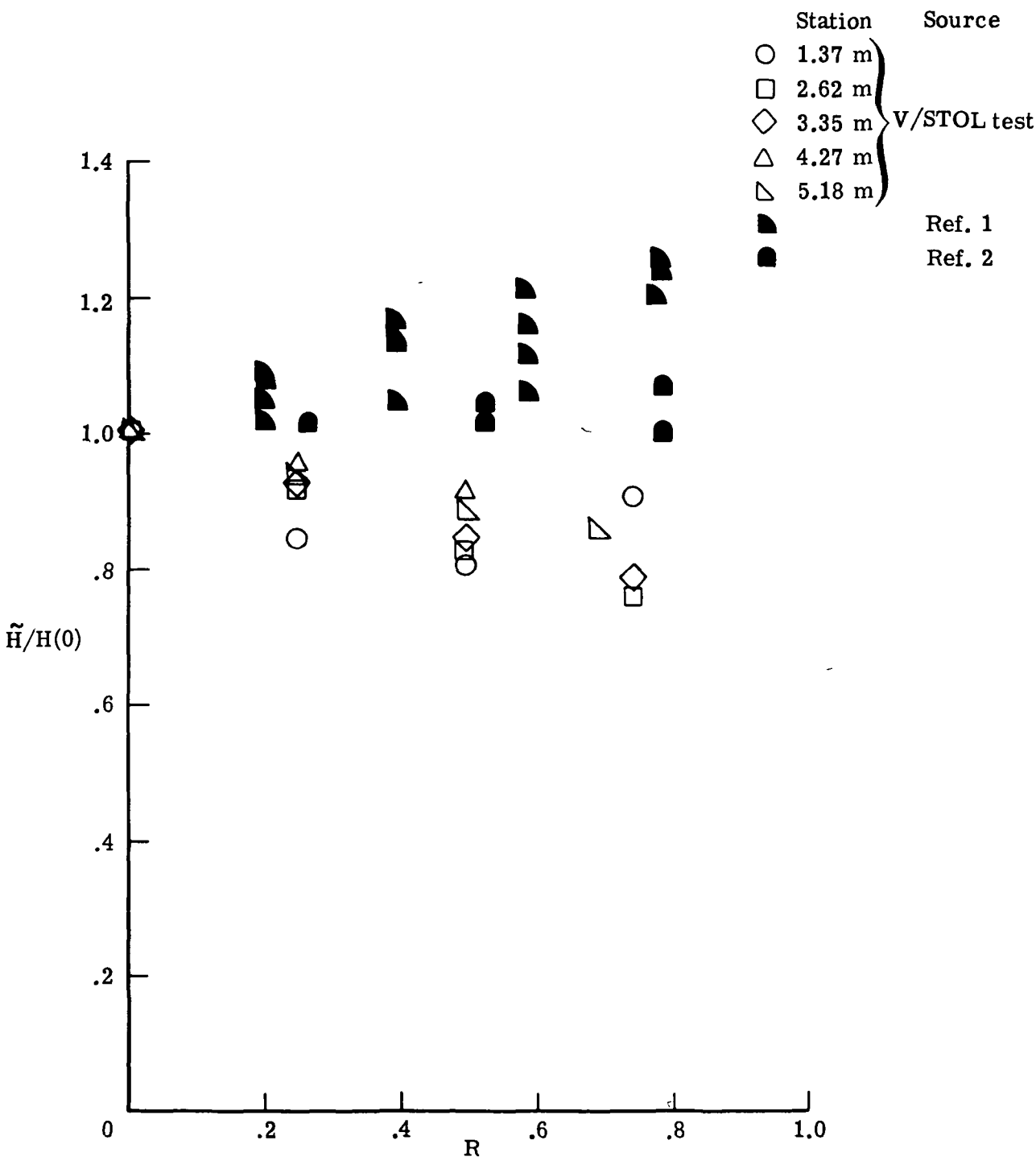


Figure 5.- Variation of relative shape factor with ground-plane speed.

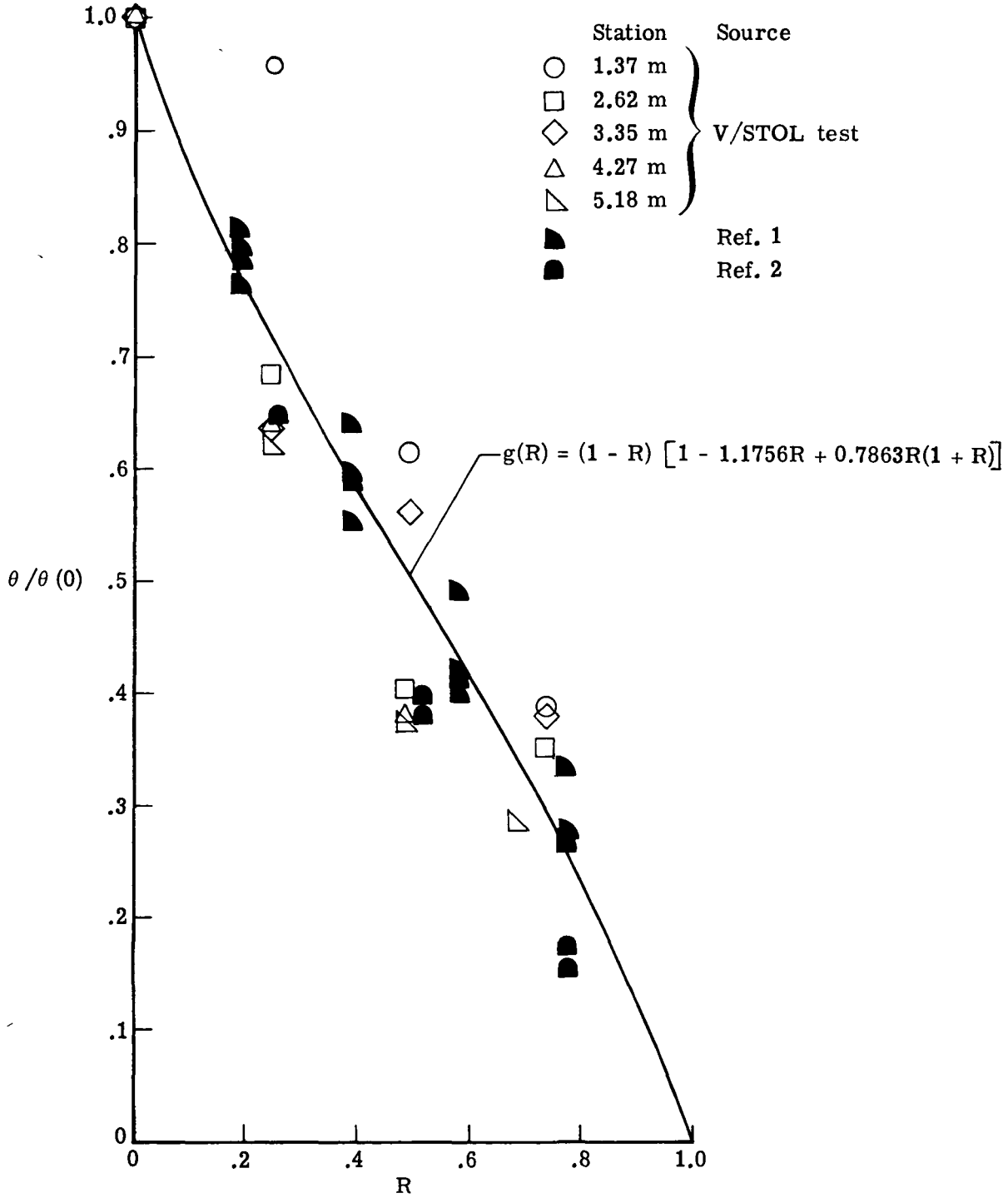


Figure 6.- Variation of $g(R) = \theta/\theta(0)$ with ground-plane speed.

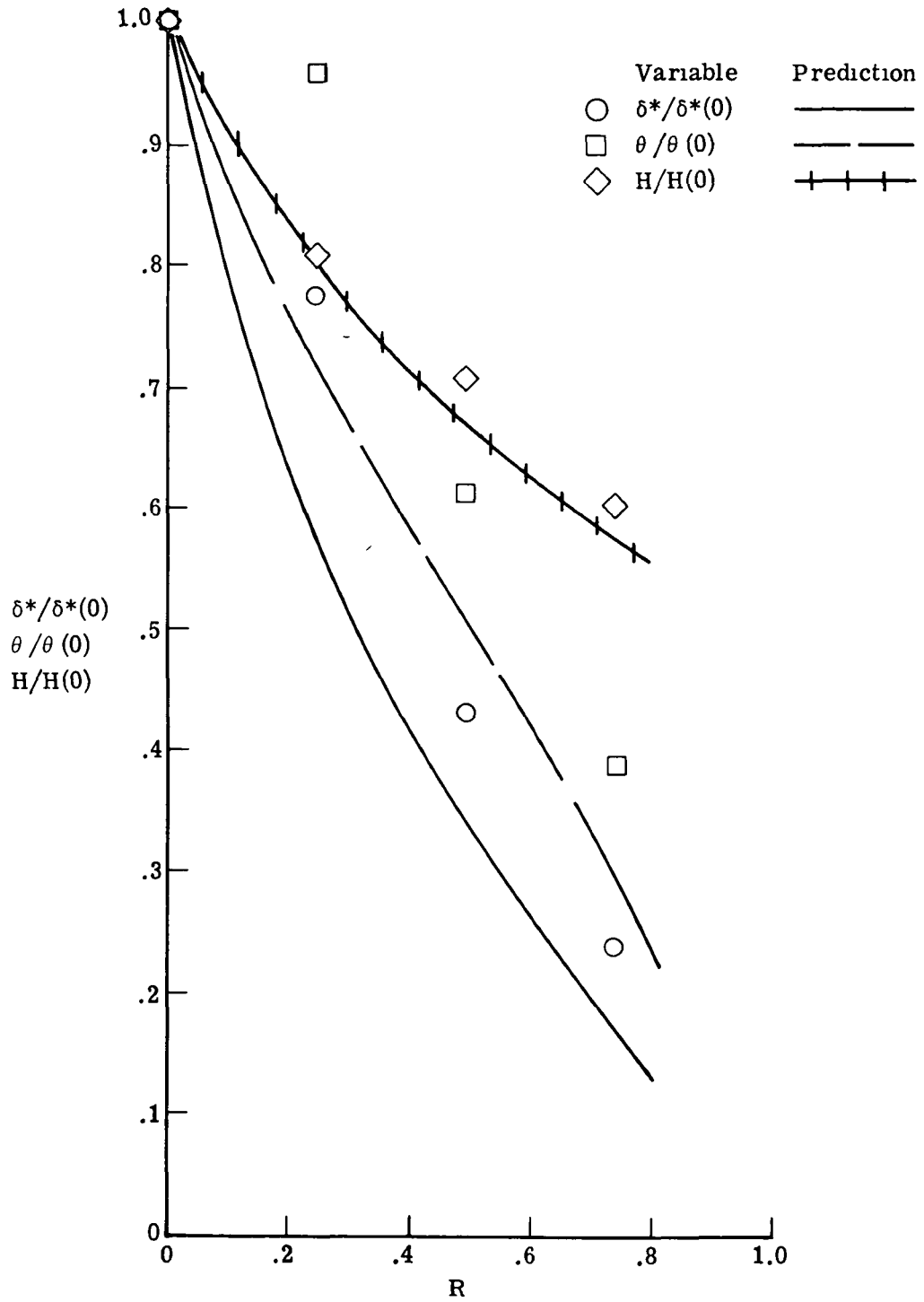


(a) Station x = 1.37 m (4.50 ft).

Figure 7.- Comparison of measured and predicted values of the integral relative integral parameter method.

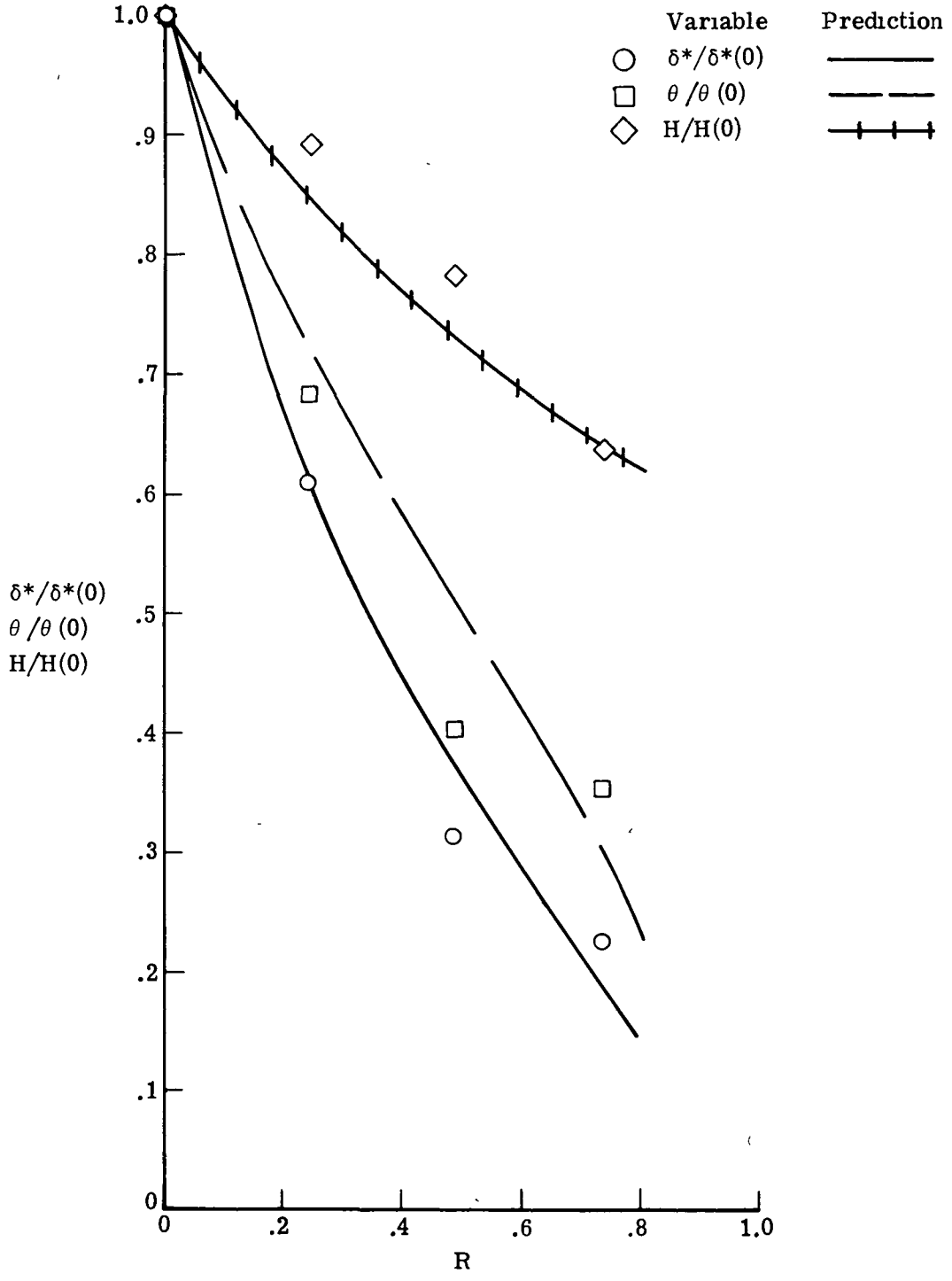


(b) Station x = 2.62 m (8.58 ft).

Figure 7.- Continued.

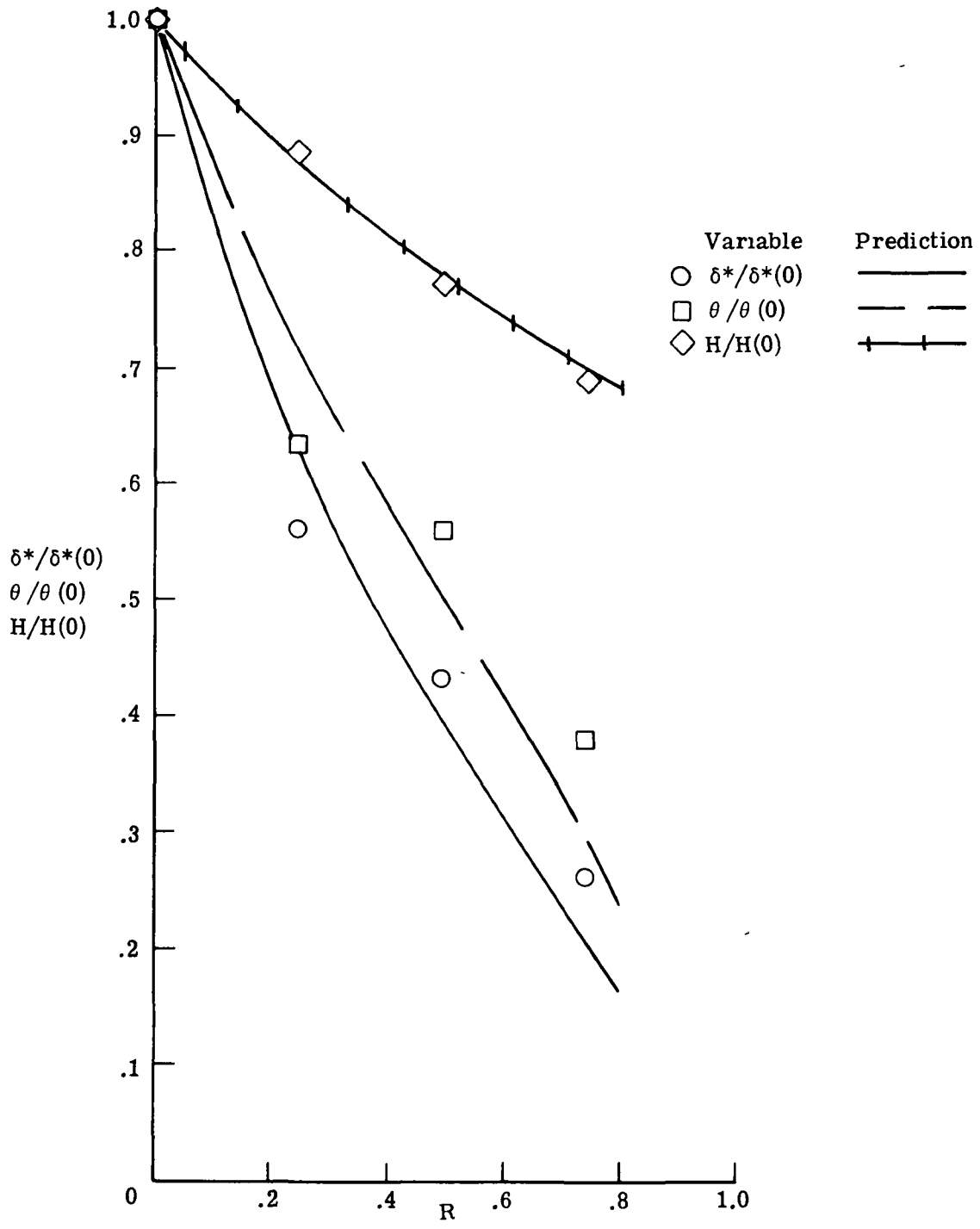


(c) Station x = 3.35 m (11.00 ft).

Figure 7.- Continued.

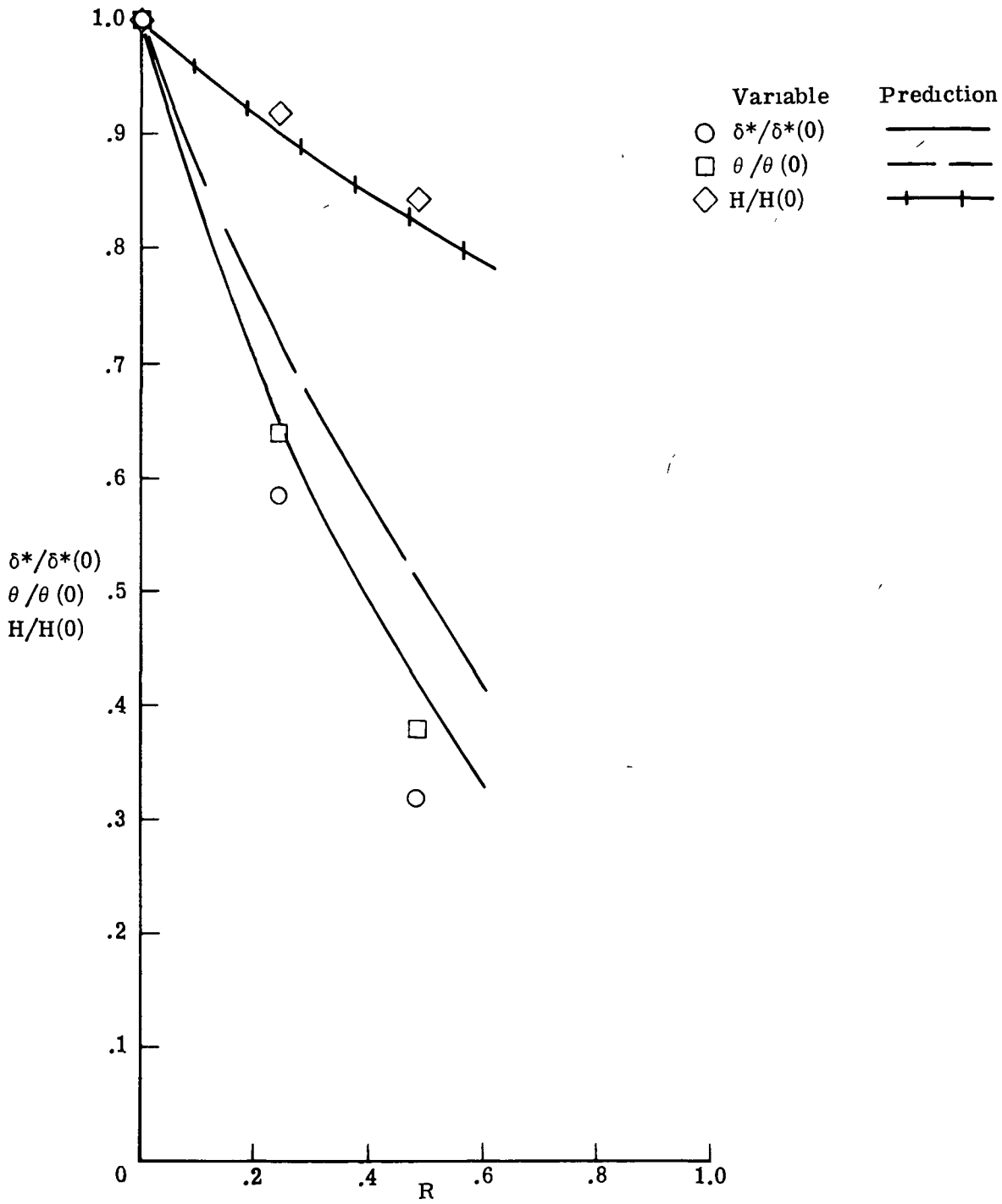


(d) Station x = 4.27 m (14.00 ft).

Figure 7.- Continued.

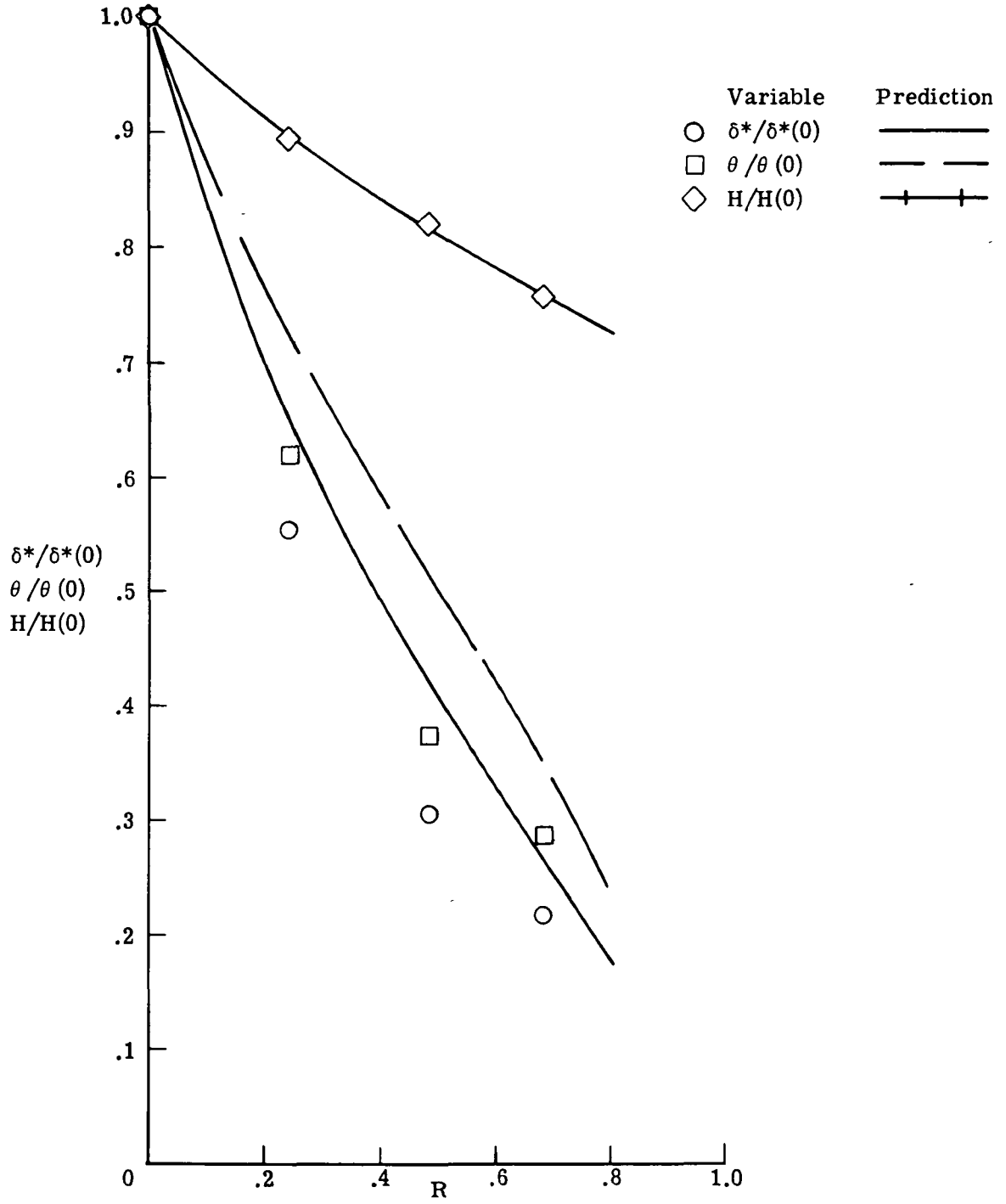


(e) Station x = 5.18 m (17.00 ft).

Figure 7.- Concluded.

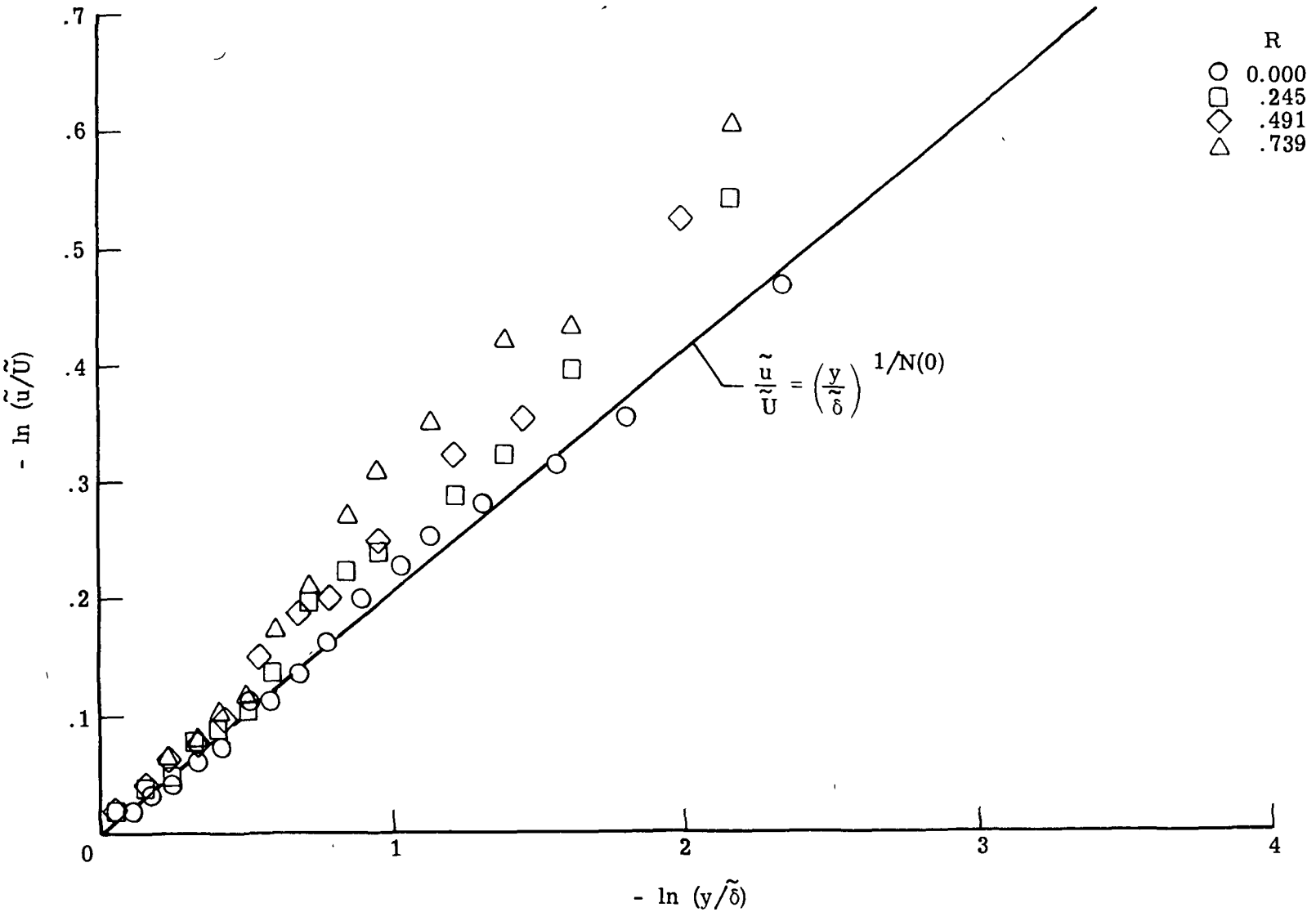


(a) Station x = 1.37 m (4.50 ft).

Figure 8.- Measured relative velocity profiles.

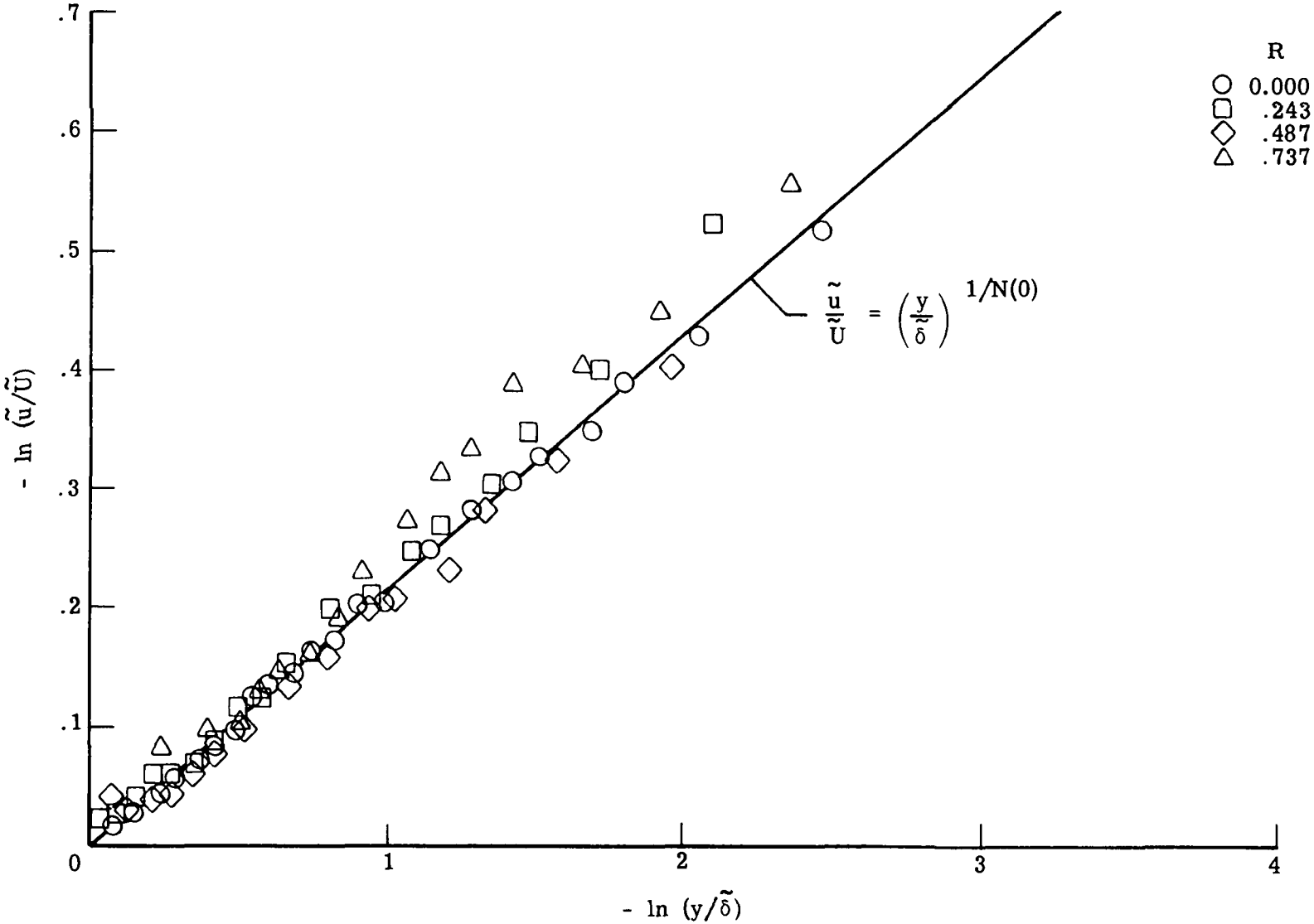


(b) Station x = 2.62 m (8.58 ft).

Figure 8.- Continued.

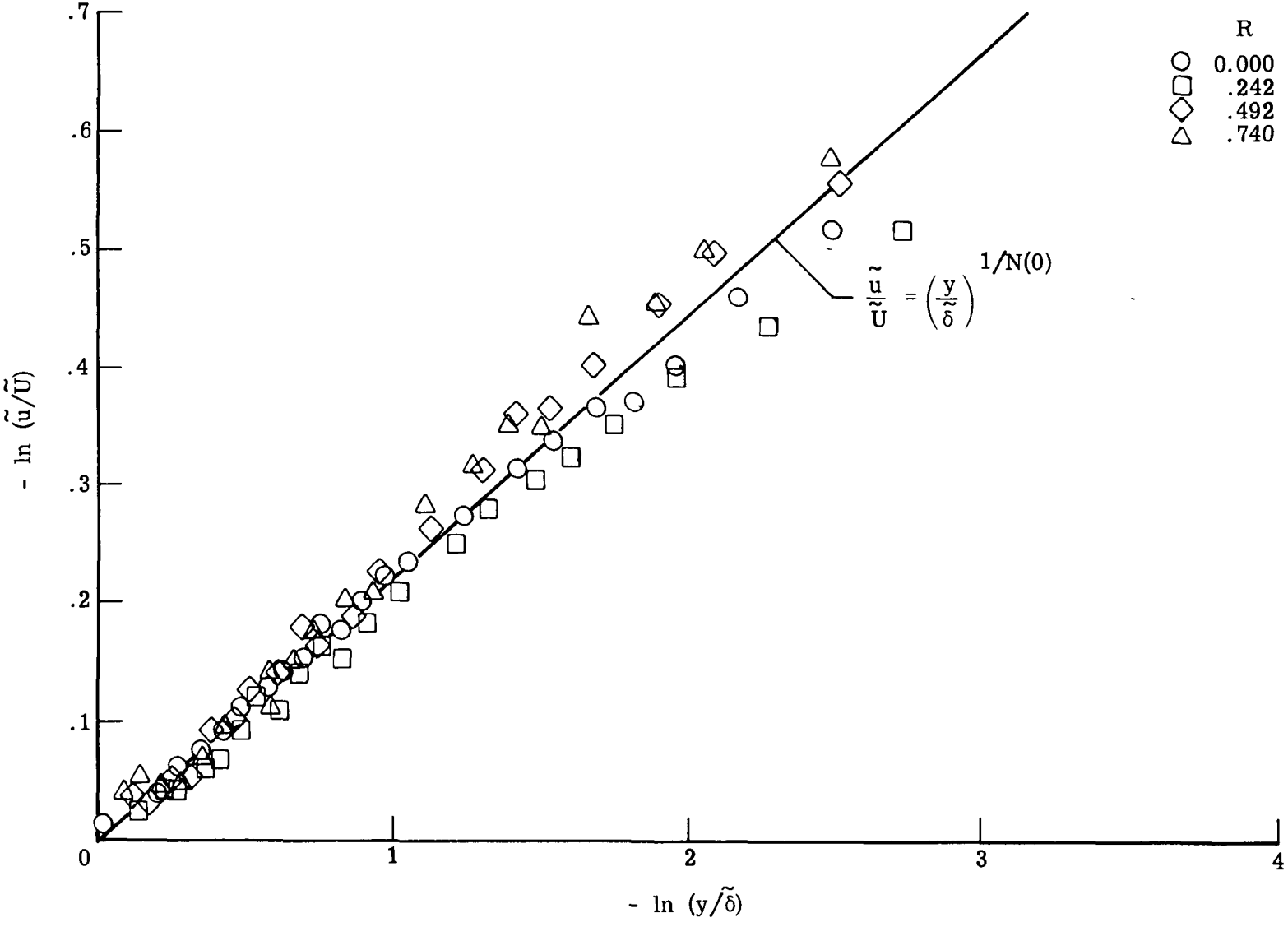


(c) Station x = 3.35 m (11.00 ft).

Figure 8.- Continued.

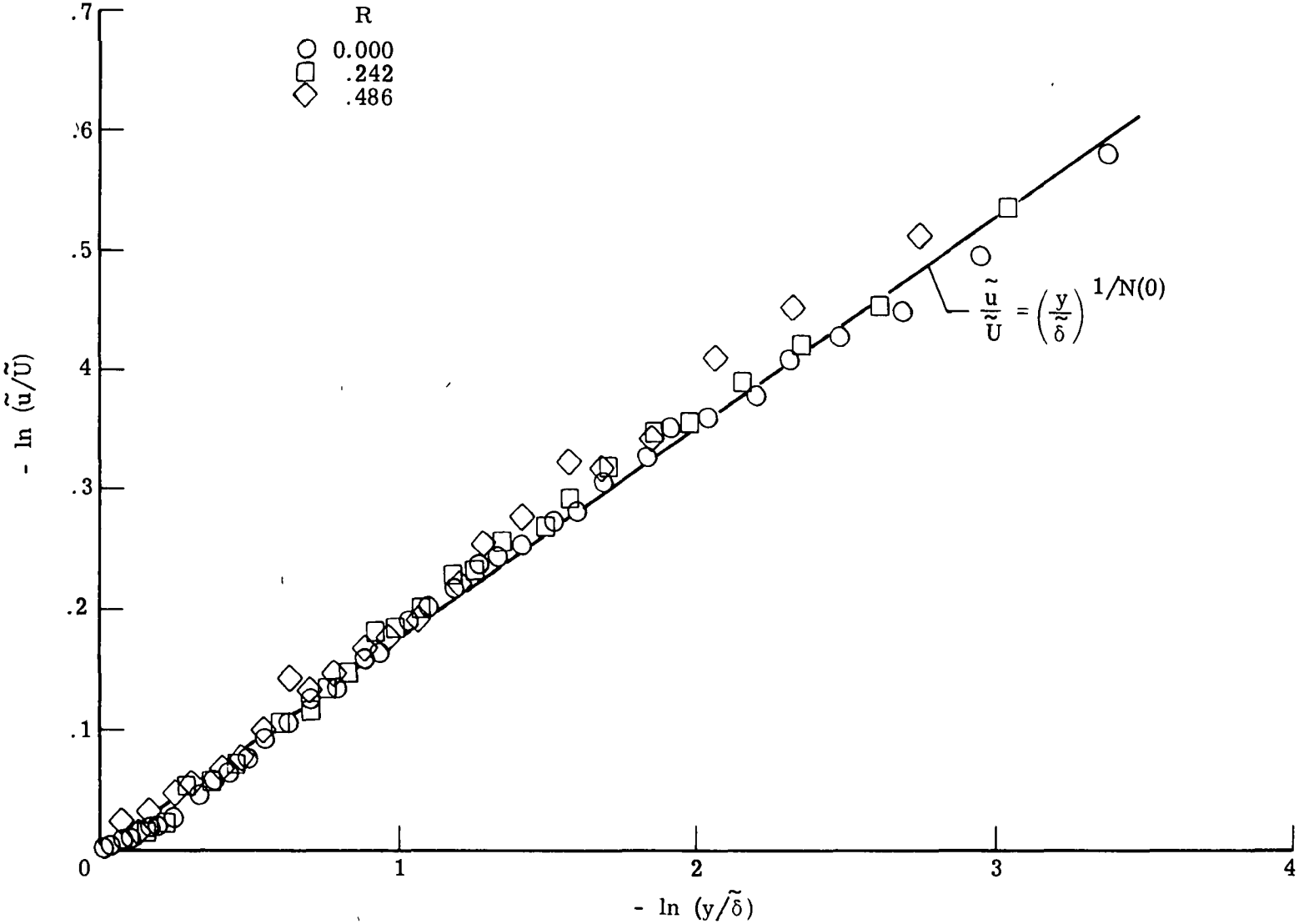


(d) Station x = 4.27 m (14.00 ft).

Figure 8.- Continued.

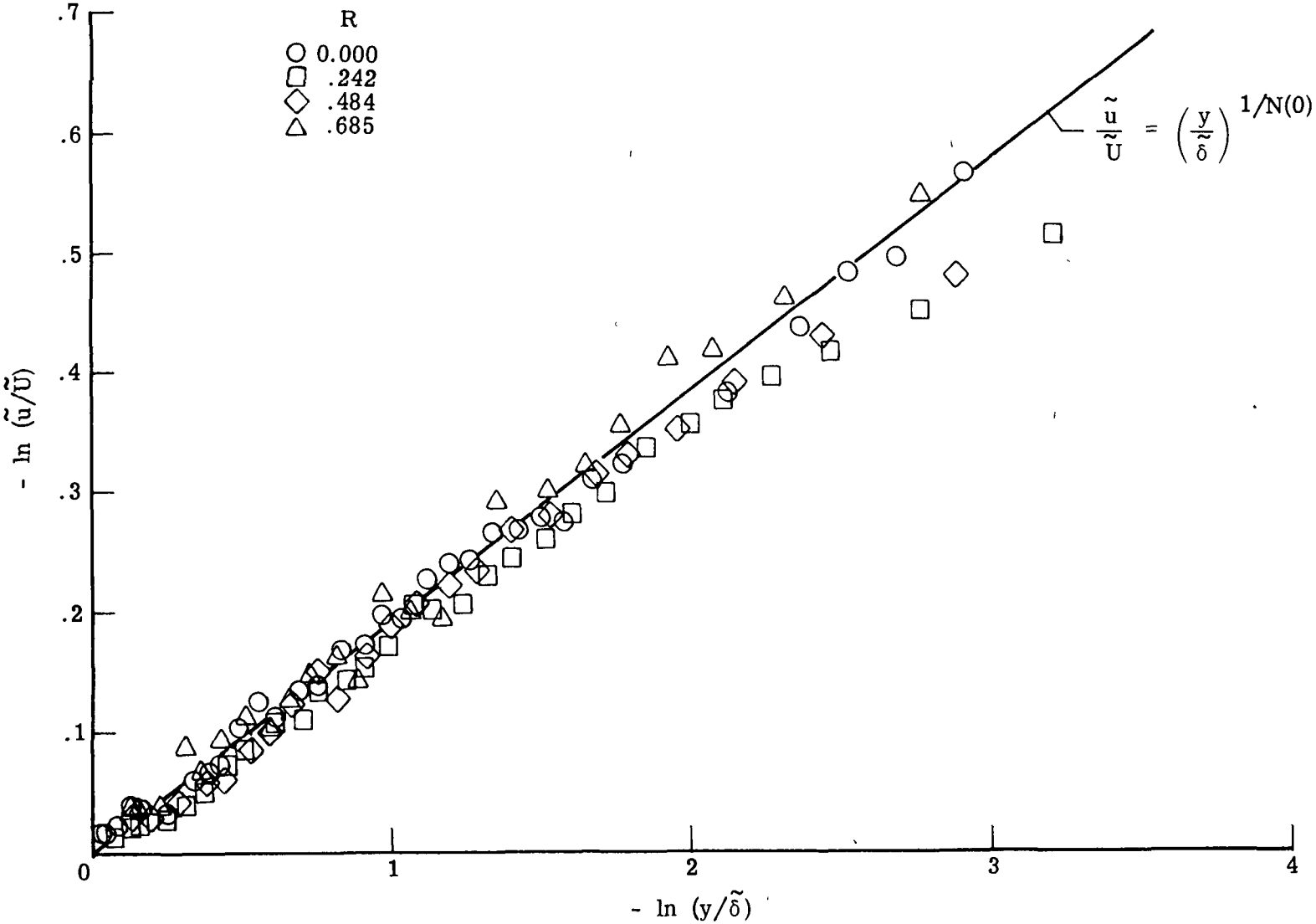


(e) Station x = 5.18 m (17.00 ft).

Figure 8.- Concluded.

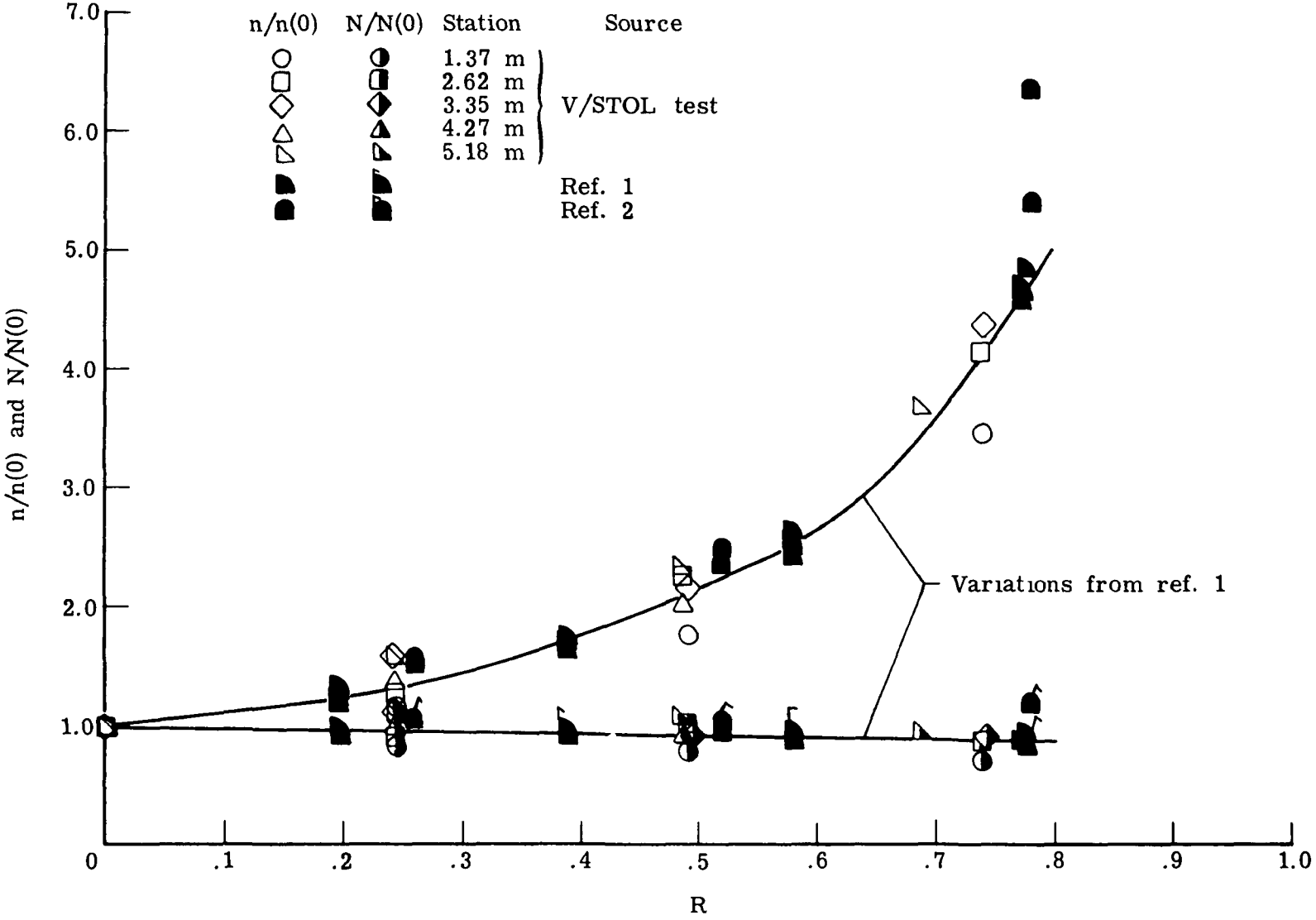


Figure 9.- Variation of n and N with belt speed.

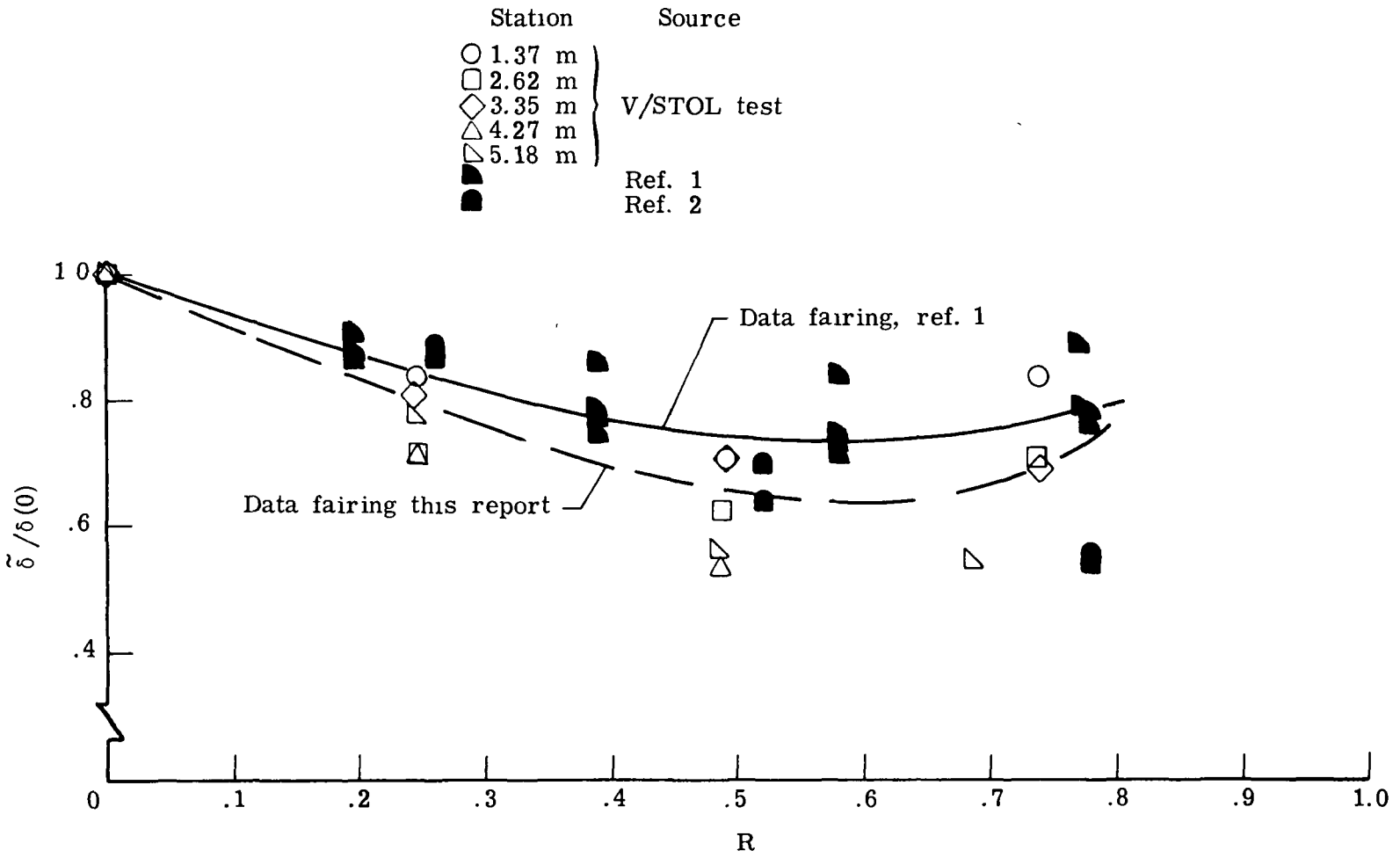


Figure 10.- Variation of relative boundary-layer thickness with ground-plane speed.

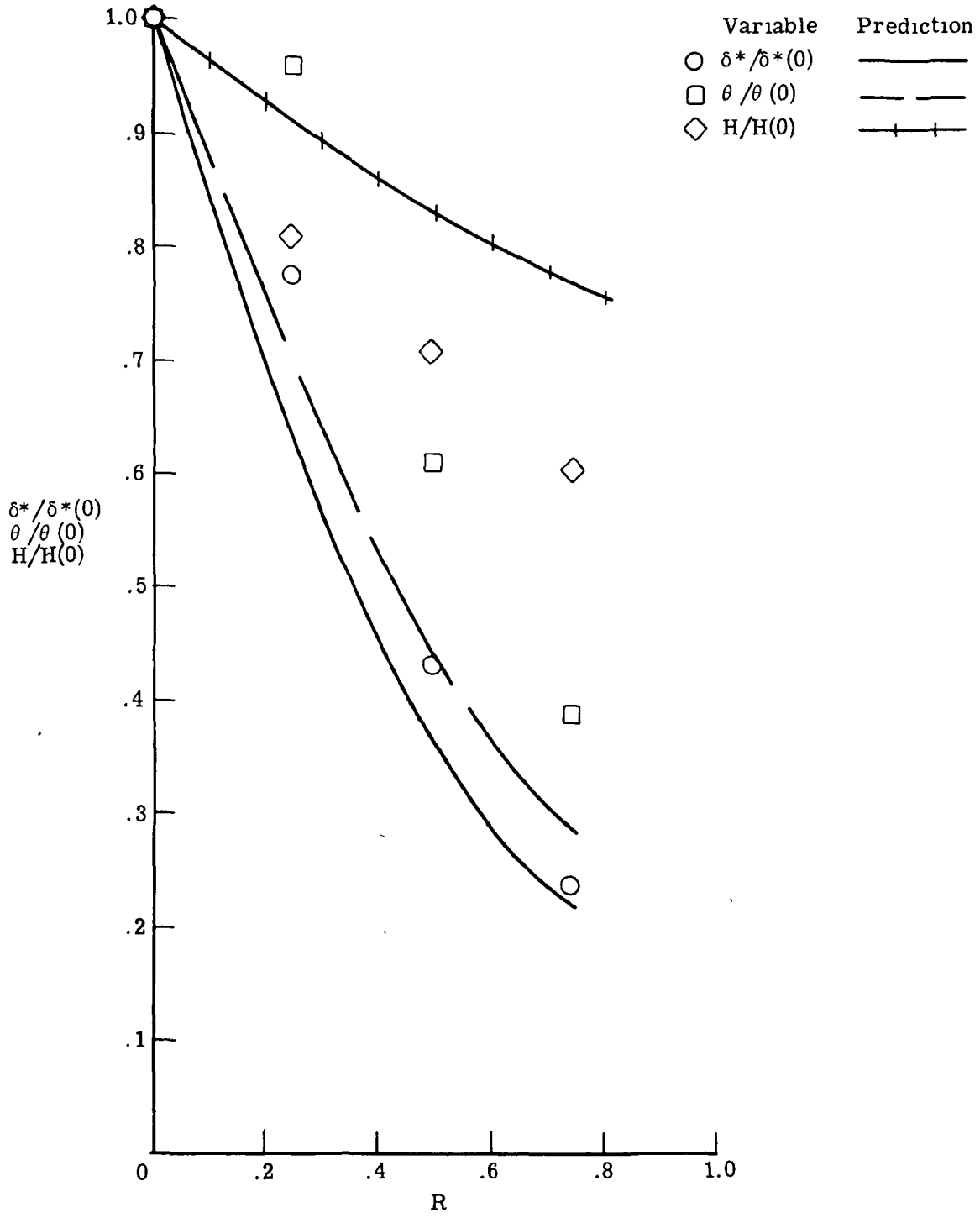


(a) Station x = 1.37 m (4.50 ft).

Figure 11.- Comparison of measured and predicted values of integral relative power law method.

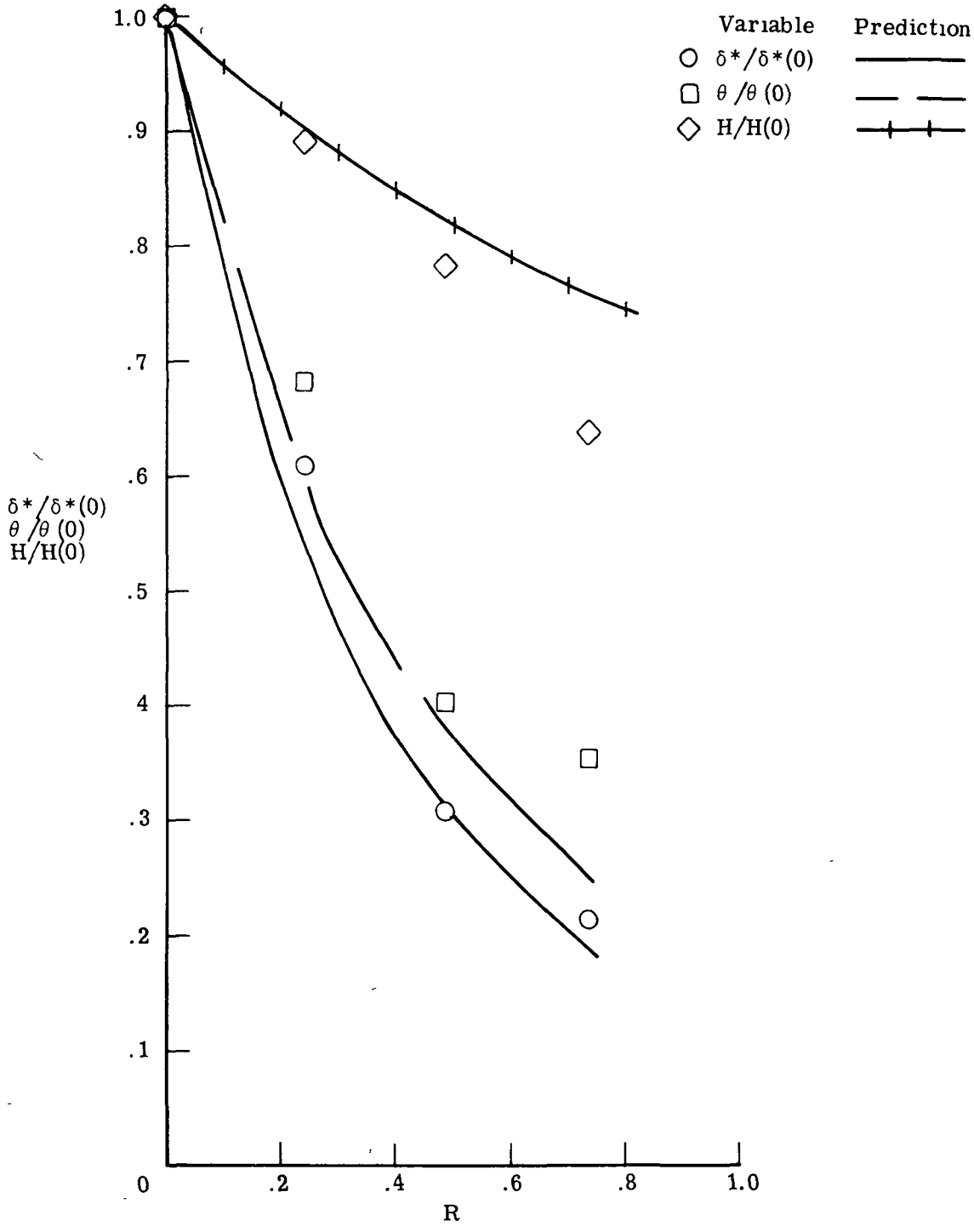


(b) Station x = 2.62 m (8.58 ft).

Figure 11.- Continued.

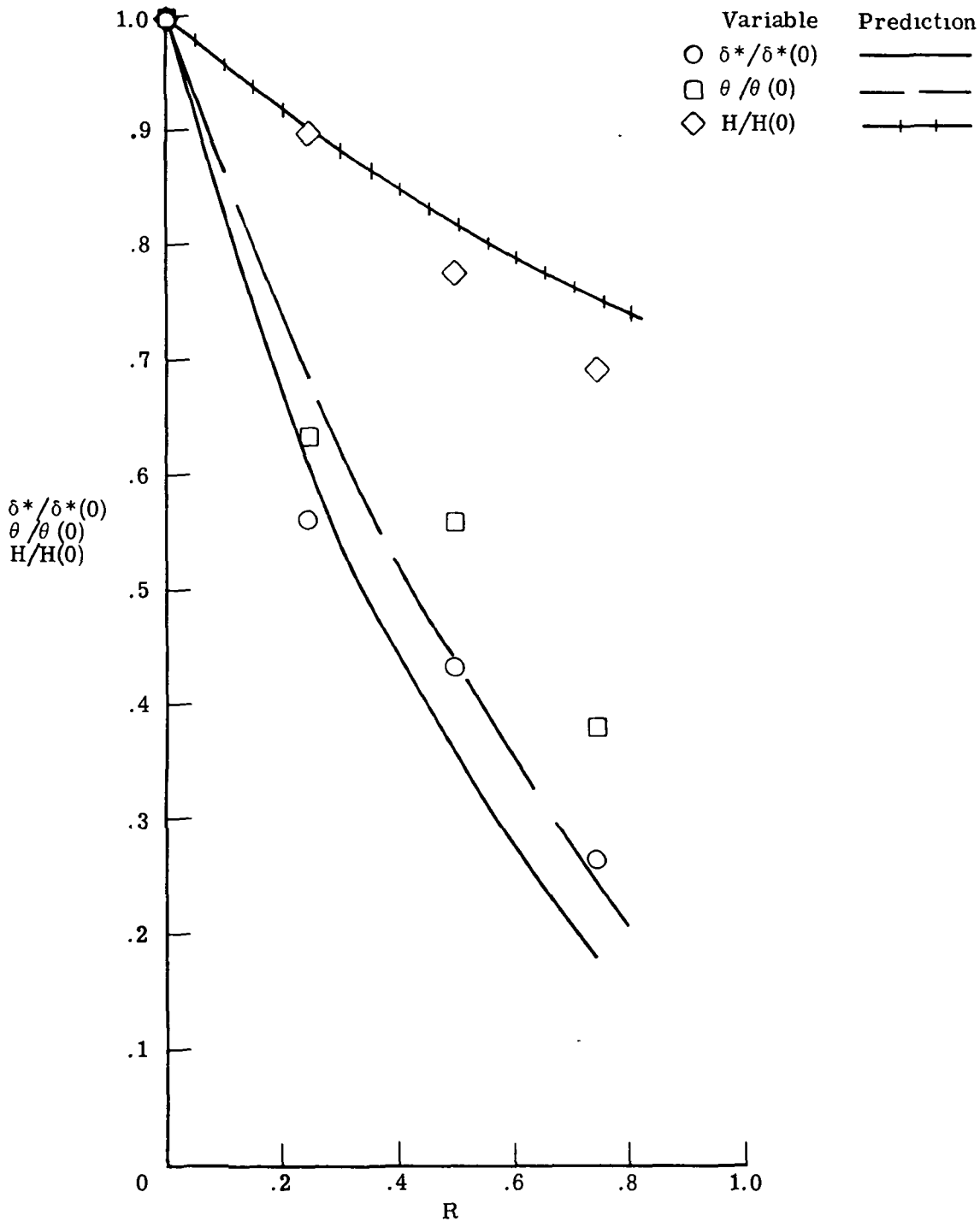


(c) Station x = 3.35 m (11.00 ft).

Figure 11.- Continued.

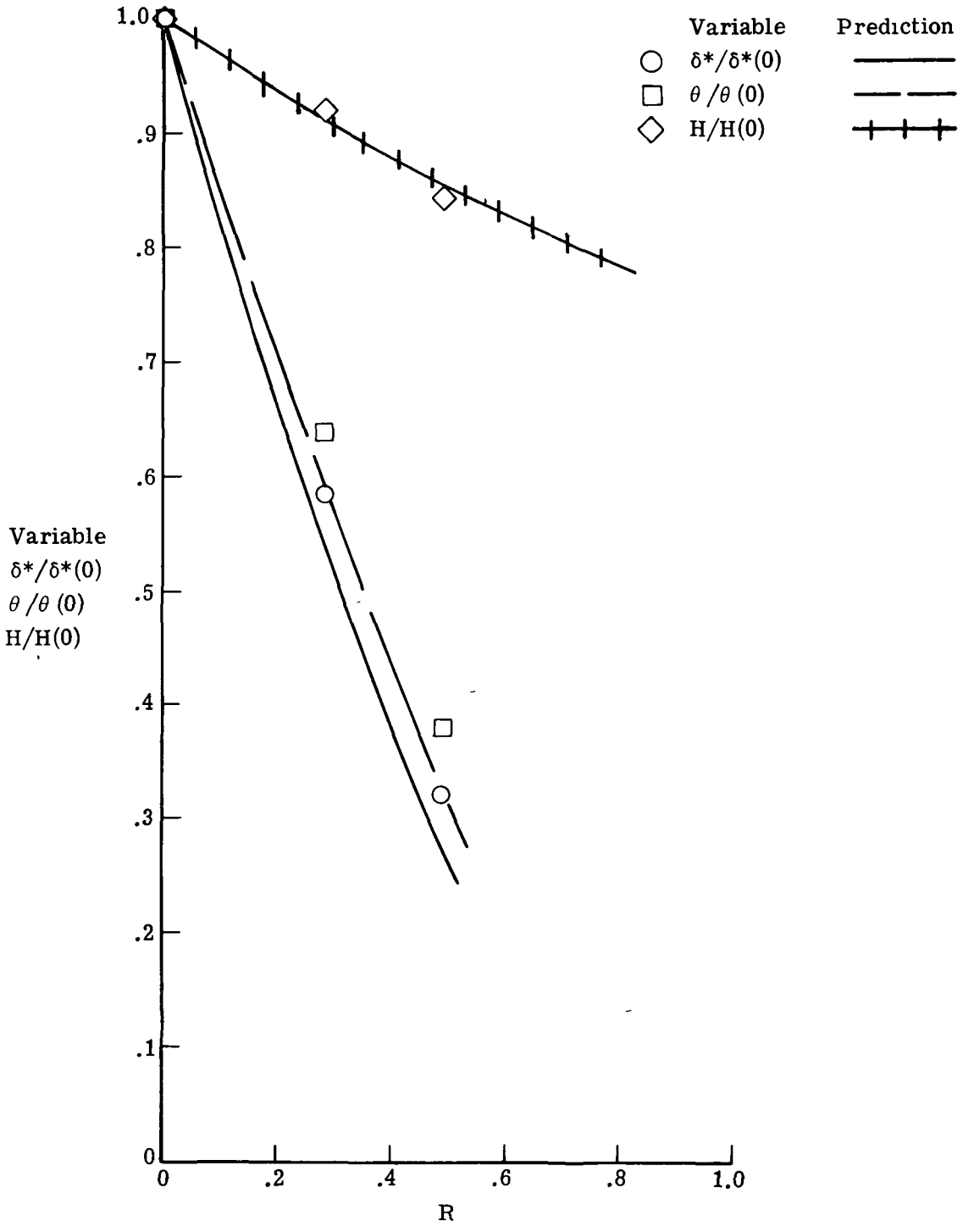


(d) Station x = 4.27 m (14.00 ft).

Figure 11.- Continued.

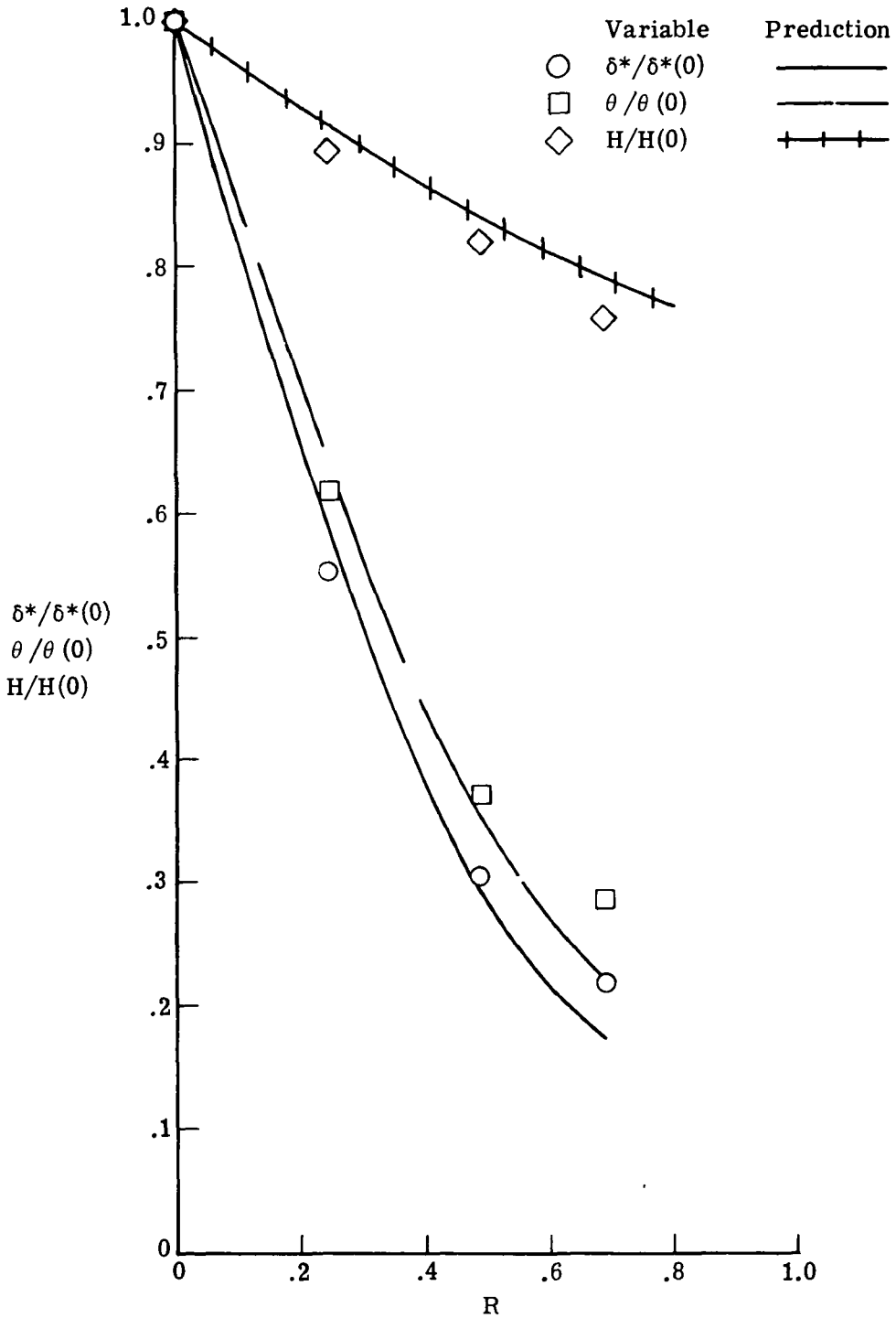


(e) Station x = 5.18 m (17.00 ft).

Figure 11.- Concluded.

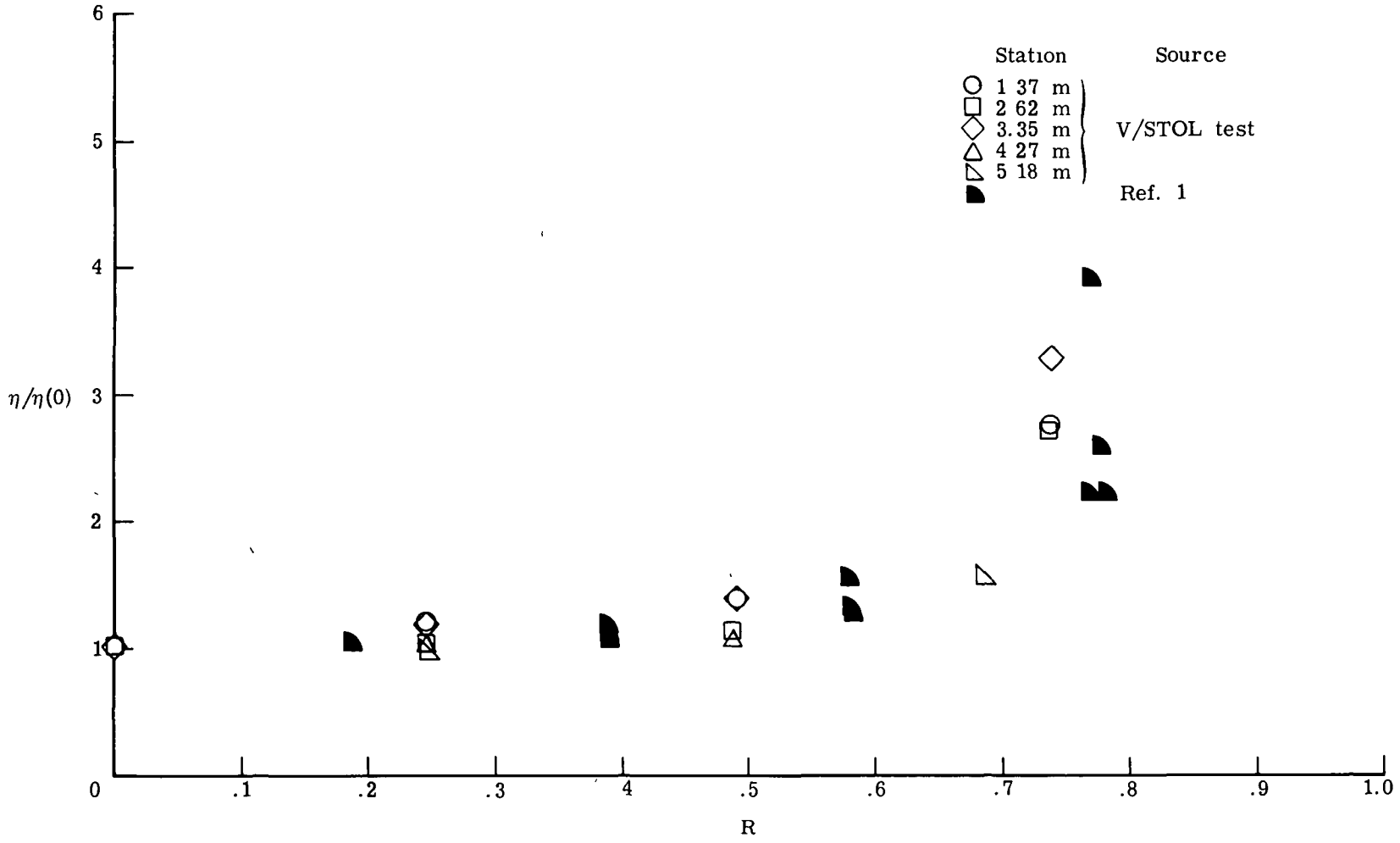


Figure 12.- Variation of reciprocal of exponent in Blasius shear stress expression as a function of ground-plane speed.

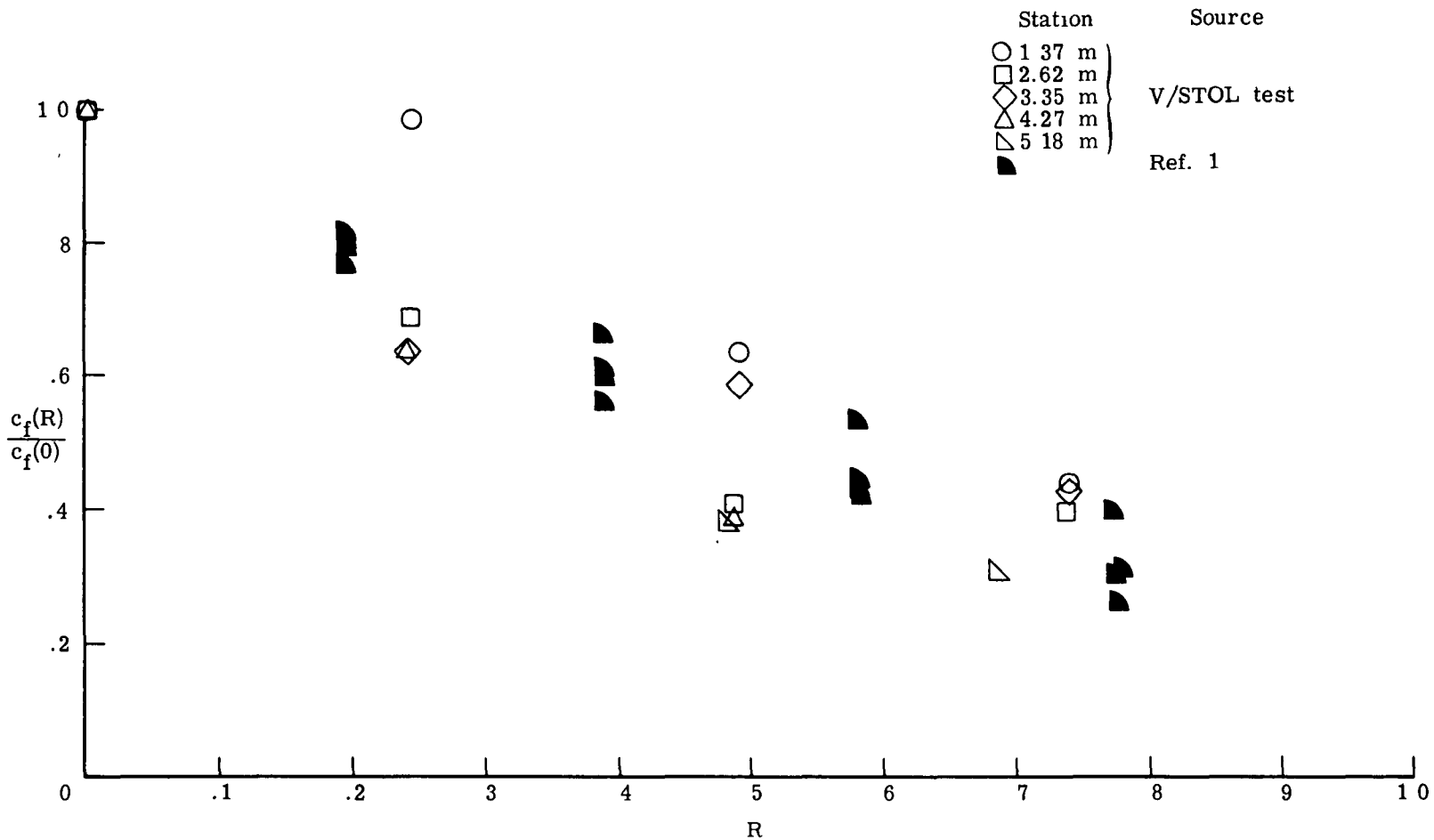


Figure 13.- Local skin-friction coefficients determined by relative power law method.

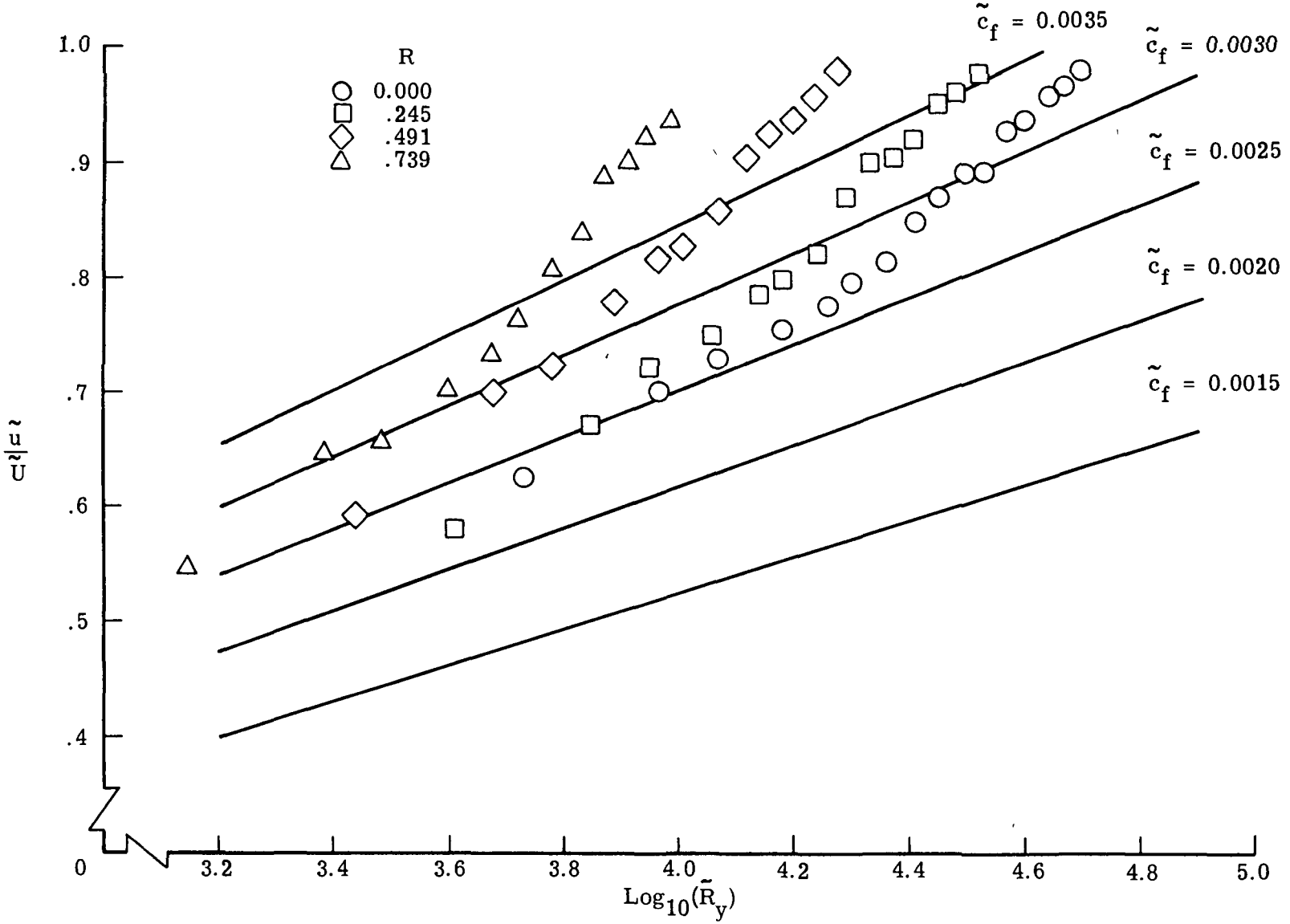


(a) Station x = 1.37 m (4.50 ft).

Figure 14.- Skin-friction coefficients determined by modified law of wall method.

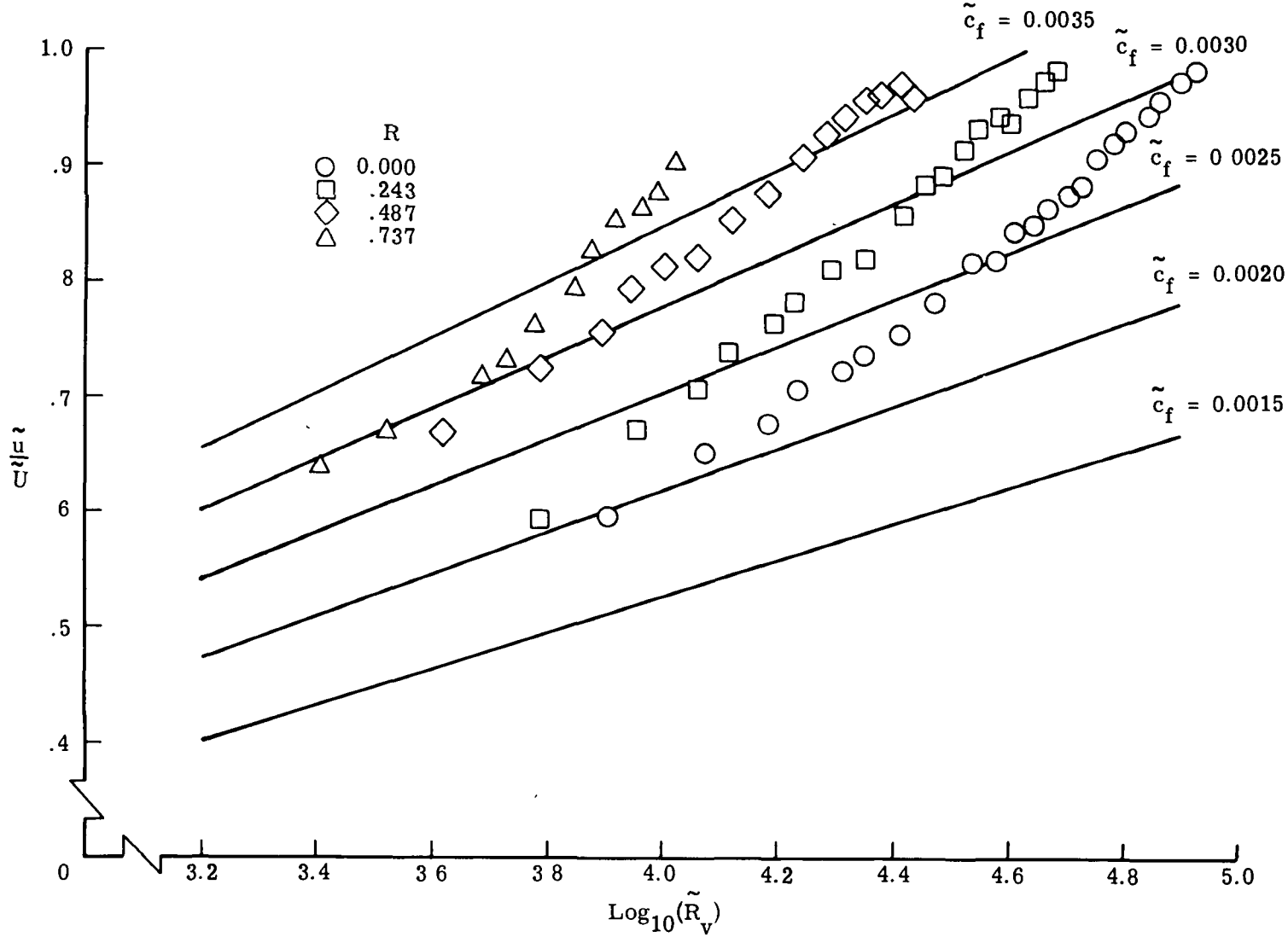


(b) Station x = 2.62 m (8.58 ft).

Figure 14.- Continued.

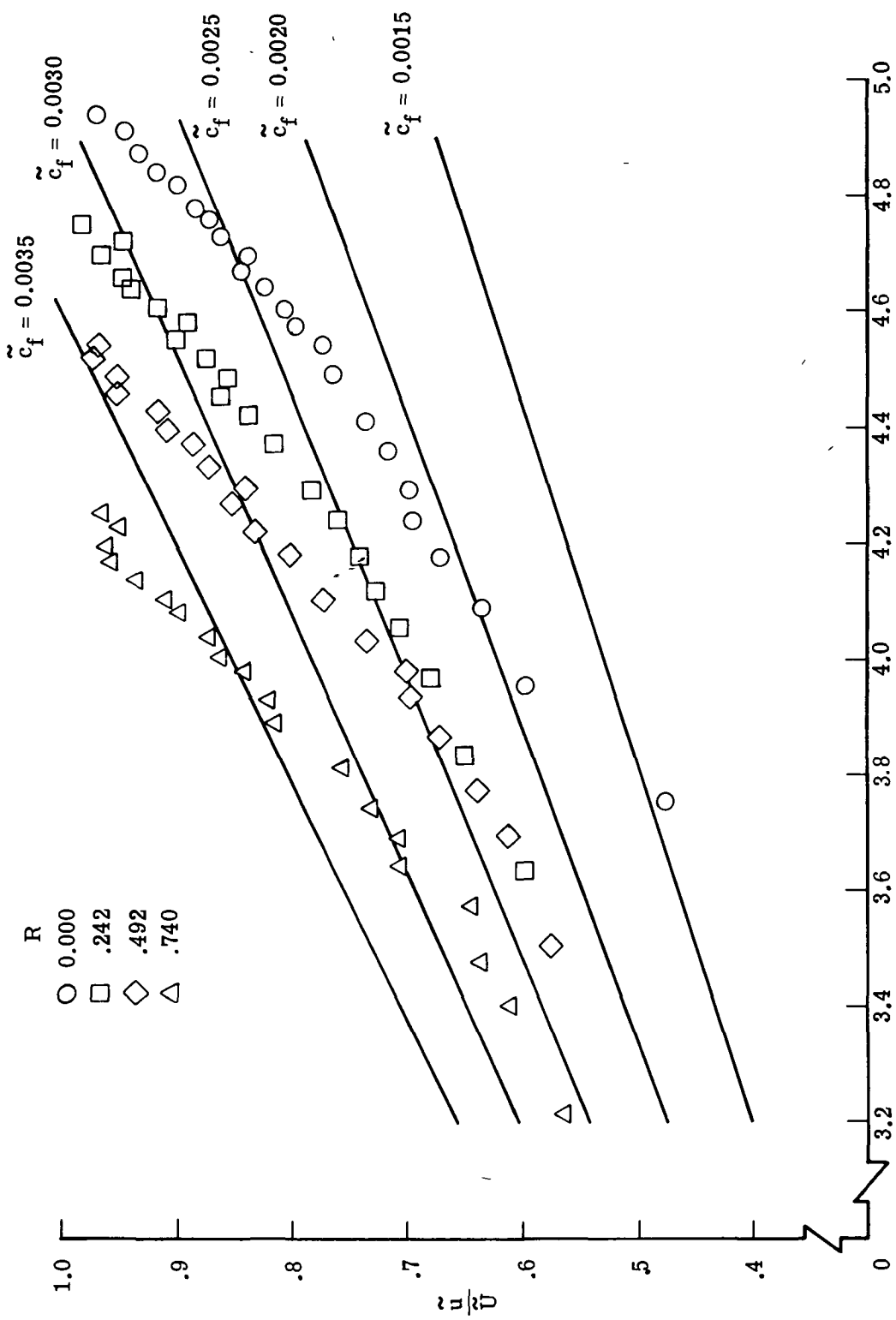


(c) Station x = 3.35 m (11.00 ft).

Figure 14.- Continued.

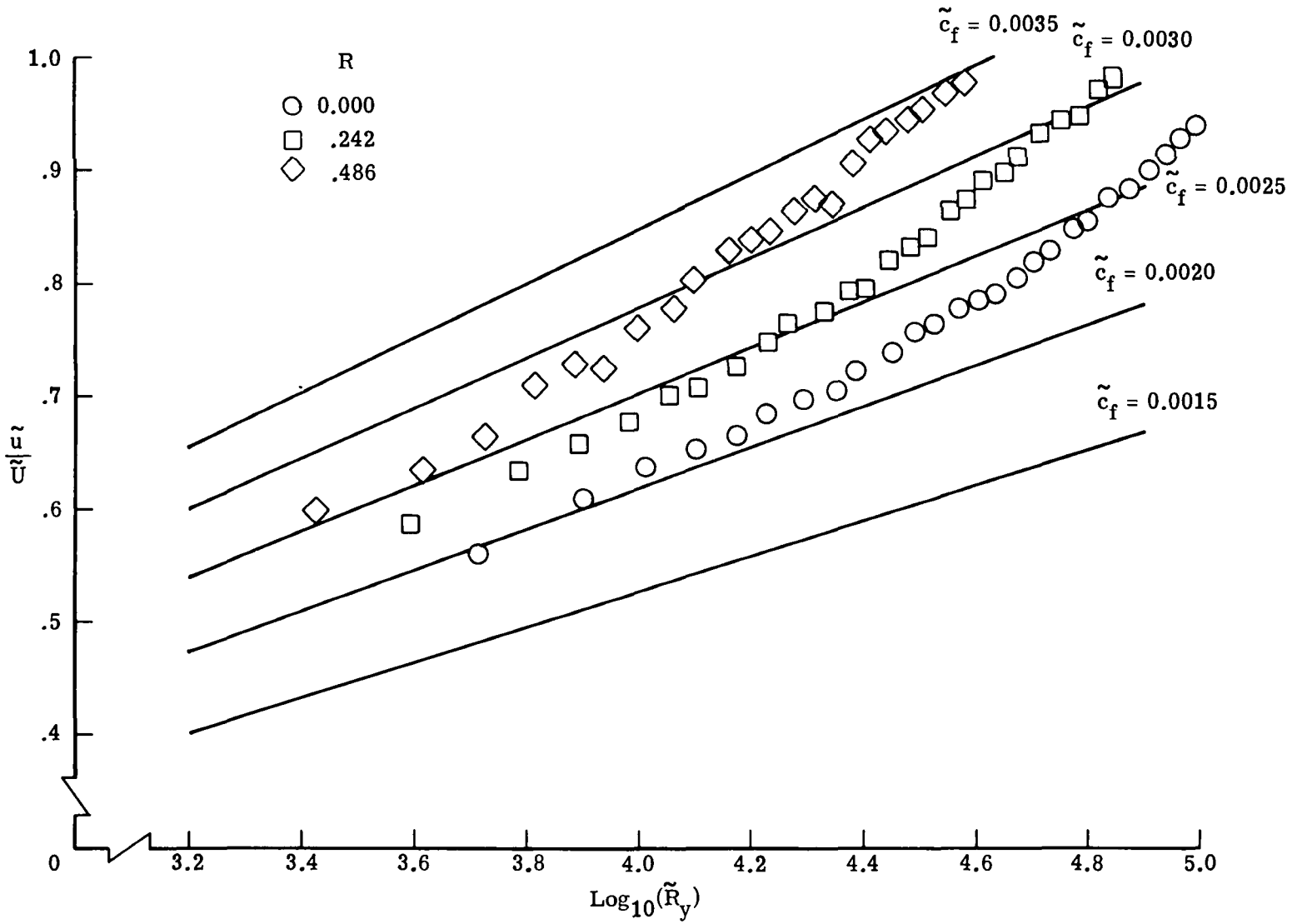


(d) Station x = 4.27 m (14.00 ft).

Figure 14.- Continued.

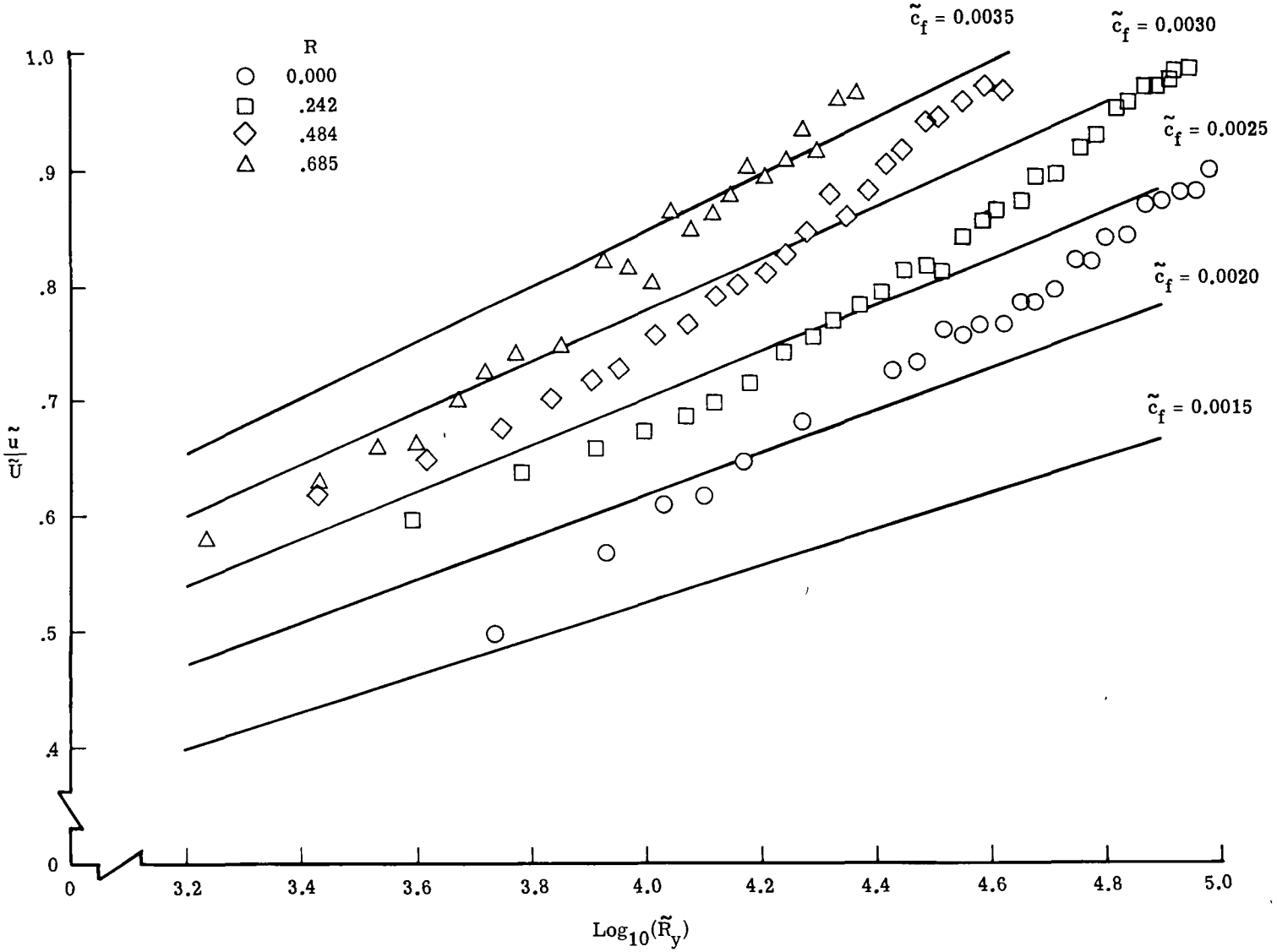


(e) Station x = 5.18 m (17.00 ft).

Figure 14.- Concluded.

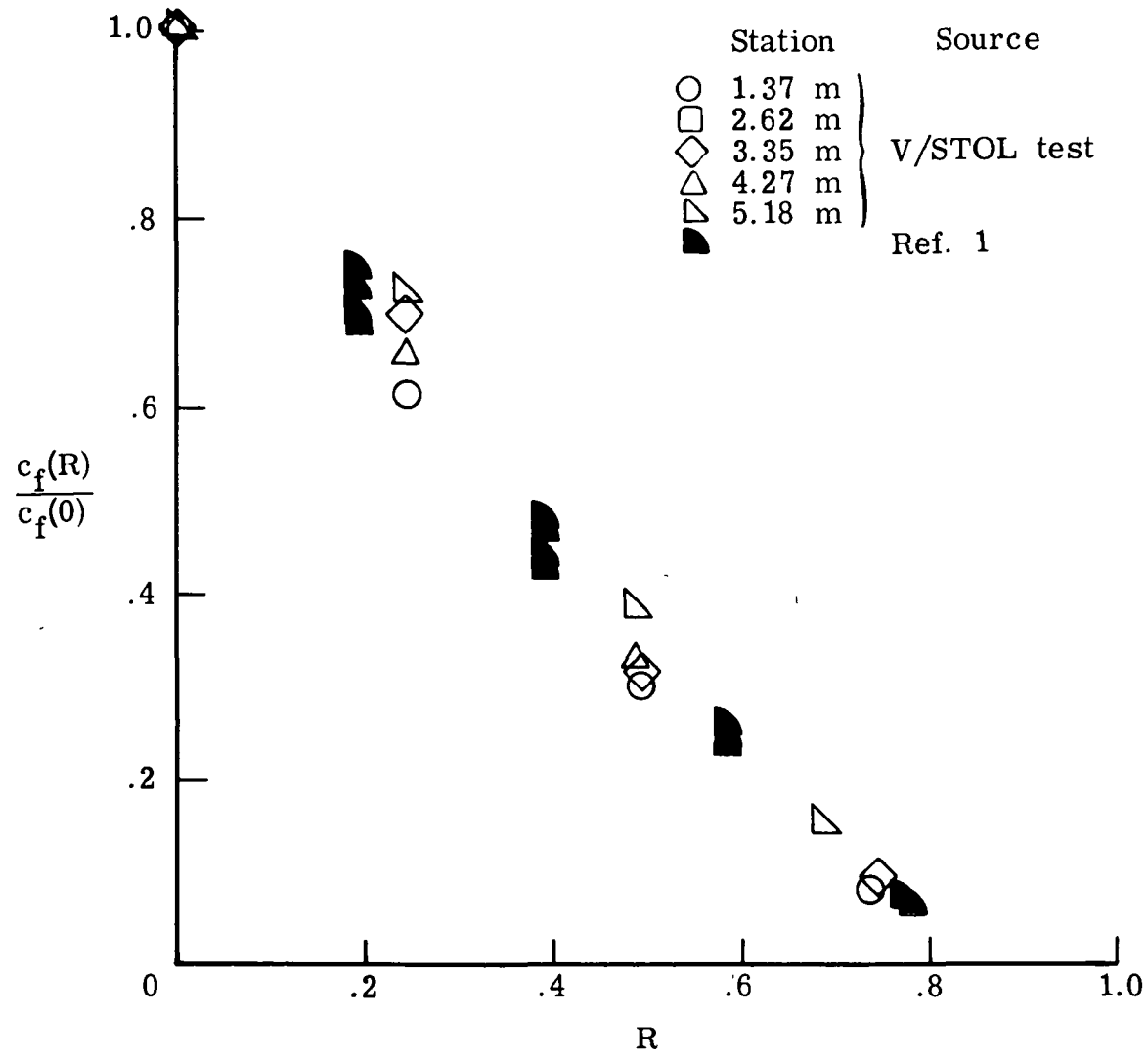


Figure 15.- Local skin-friction coefficients determined by the modified law of wall method.

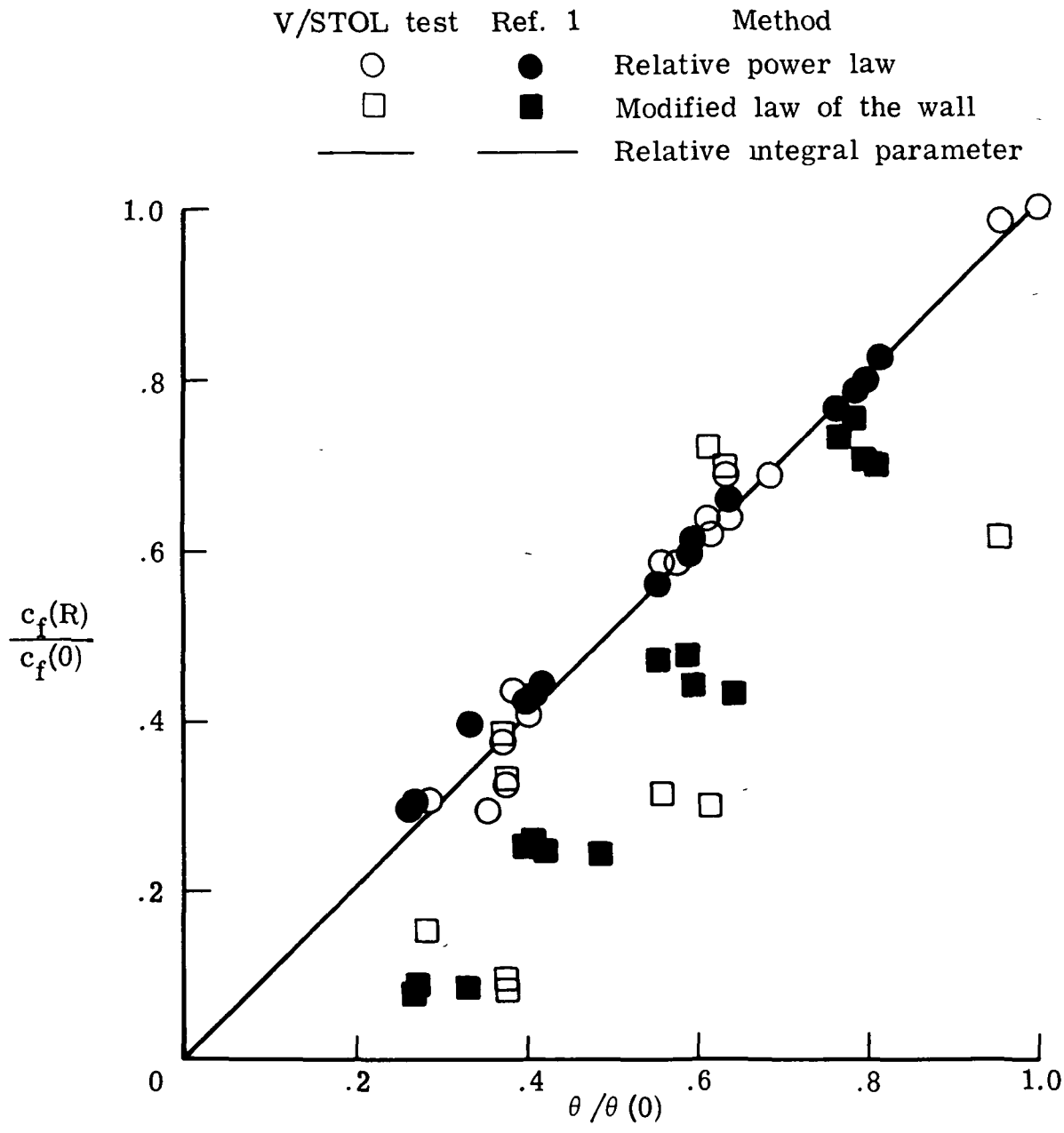


Figure 16.- Comparison of local skin-friction coefficients determined by relative integral parameter method, relative power law method, and modified law of wall method.

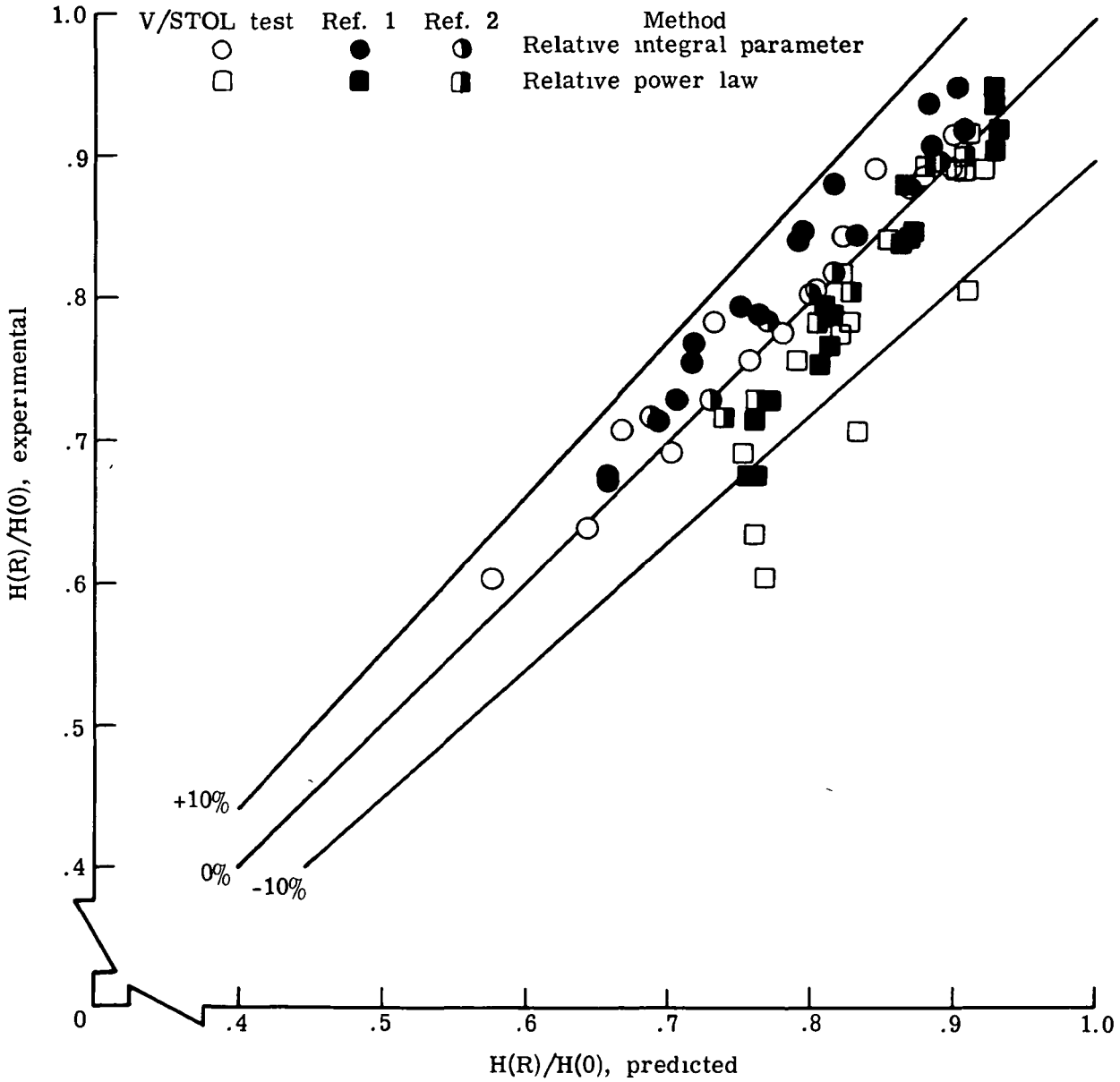


Figure 17.- Comparison of values of H(R)/H(0) predicted from relative integral parameter and relative power law methods with experimental data.

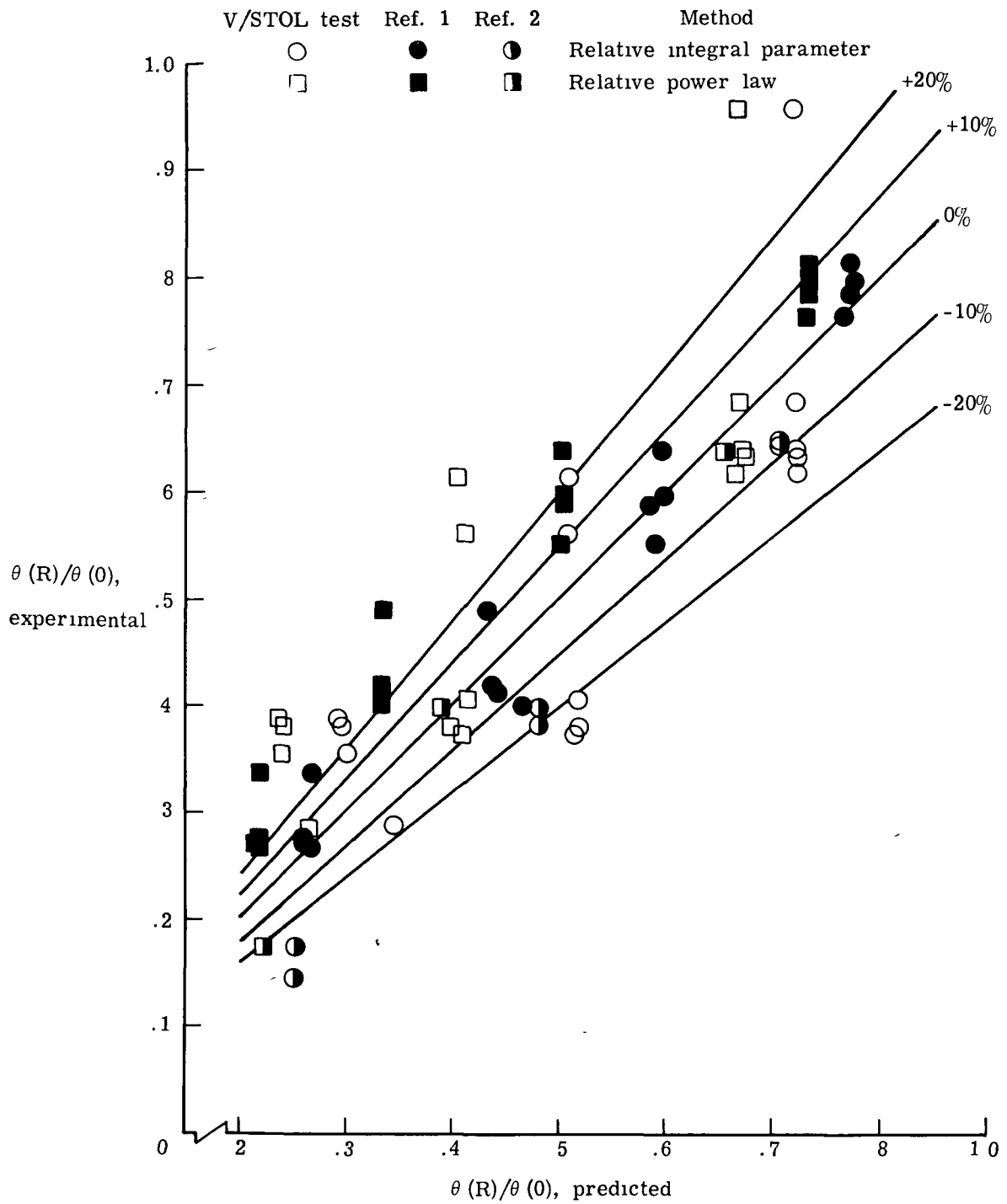


Figure 18.- Comparison of values of θ(R)/θ(0) predicted from relative integral parameter and relative power law methods with experimental data.

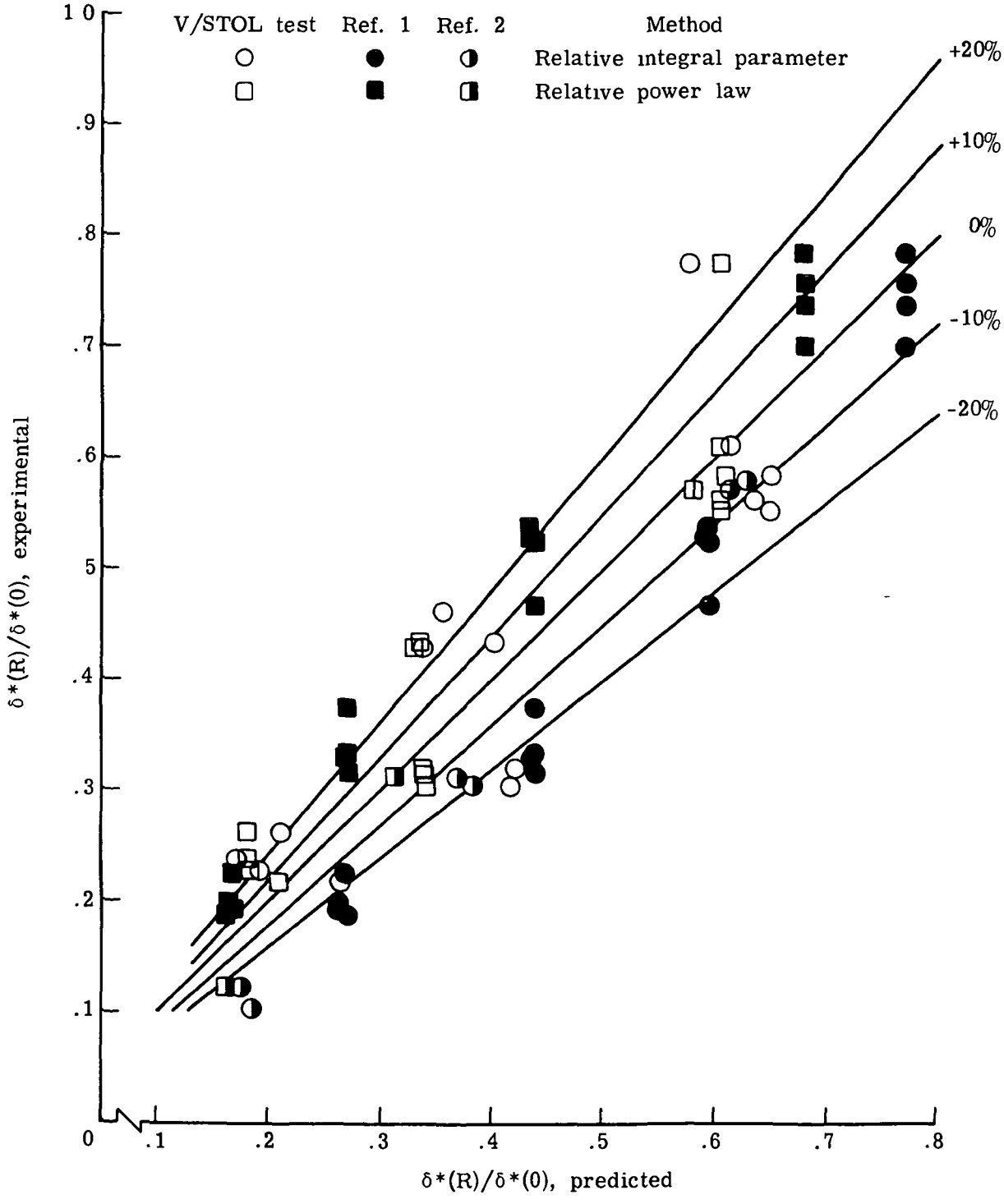


Figure 19.- Comparison of values of $\delta^*(R)/\delta^*(0)$ predicted from relative integral parameter and relative power law methods with experimental data.